# Including the Angular Domain in the Analysis of Finite Multi-Packet Peer-to-Peer Networks With Uniformly Distributed Sources

Fulvio Babich, *Senior Member, IEEE*, and Massimiliano Comisso, *Member, IEEE*

***Abstract*— This paper presents a mathematical framework for including the angular domain beside the radial one in the theoretical modeling of wireless networks, in which spatial reuse enables the coexistence of multiple single-hop peer-to-peer communications inside a finite region. The proposed model analyzes a scenario where the transmitting sources are uniformly distributed over a disk and the communications are subjected to path-loss attenuation and multipath-fading, considering the actual location of each destination and its antenna system. Different from most of the previous theories in which the coverage probability of a destination is estimated assuming that the destination itself is positioned at the center of the network, in the proposed analysis, the destination location is generic. This generalization, together with the consideration of the spatial channel model and of the actual receiving pattern, allows one to investigate the influence of the angular domain on the statistic of the interference power and on the coverage probability. The conceived theory, which is further verified by Monte Carlo validations, is finally exploited to derive the network transmission capacity, with the purpose to illustrate the possible advantages that may derive from a reliable modeling of the non-isotropic context, in which each destination has to operate realistically.**

***Index Terms*— Wireless network, multi-packet, peer-to-peer, angle, interference, transmission capacity.**

## I. Introduction

THE ANALYTICAL characterization of the result of a communication attempt in a wireless network has always represented a relevant research topic, since the continuous development of novel access strategies and physical layer technologies has required the extension of the existing theories to include the most recent advances. In particular, the exploitation of the spatial domain for allowing massive access opportunities to multiple users has introduced a very challenging scenario, in which the interference model plays a key role in determining the error probability for each communication. Within this field, many efforts have been first devoted to study two diffused multi-packet strategies: multi-packet transmission (MPT) [1], and multi-packet reception (MPR) [2], [3]. The former one concerns the transmission of different packets from a unique source to multiple destinations, while the latter one aims to enable a unique destination to receive packets from multiple sources at the same time. Recently, beside the MPT/MPR approaches, the increased interest towards massive access has involved also the not centralized schemes, with the purpose to enable multiple uncoordinated communications between different node pairs [4].

Manuscript accepted April 10, 2016. This work is partly supported by the Italian Ministry of University and Research (MIUR) within the project FRA 2015 (University of Trieste, Italy), entitled "Peer-to-peer Millimeter-Wave Communications in 5G Networks: Theoretical Modeling and Algorithms for Massimo MIMO Systems." The associate editor coordinating the review of this paper and approving it for publication was Z. Zhang.

The authors are with the Department of Engineering and Architecture, University of Trieste, Trieste 34127, Italy (e-mail: babich@units.it; mcomisso@units.it).

### A. Related Work

The estimation of the result of a transmission attempt in a peer-to-peer network characterized by multi-packet capabilities requires a reliable modeling of all the elements involving the spatial domain: the node location, the spatial channel model, and the antenna processing technique. The analysis of the impact of the geometry of the users on the network performance is usually carried out considering a homogeneous Poisson point process (PPP) to model the spatial distribution of the nodes. The PPP-based approach enables the derivation of sophisticated theoretical models for analyzing the interference in wireless networks, with the purpose to evaluate the error probability for each communication and the related performance metrics [5]–[14]. In particular, a useful metric, initially proposed in [5], is the transmission capacity, which identifies, for a given outage constraint, the product between the maximum spatial density of the successful transmissions and their spectral efficiency. This metric, which quantifies the area spectral efficiency of a network, has been subsequently applied to study the benefits of successive interference cancellation in wireless ad-hoc scenarios where the users are located according to a PPP [6]. The impact of spatial filtering and interference cancellation in a Poisson field of interferers for both uniform and non-uniform node densities has been investigated in [7], where directional antennas and direction of arrivals (DOAs) are modeled introducing a novel statistical selectivity parameter. A Poisson field of interferers is also assumed in [8] and [9], where the effects of path-loss attenuation, fading, shadowing, and modulation scheme are included in the analysis of the channel capacity and of the spectral outage probability. The definition of transmission capacity has been reformulated in [10] to account for the interference correlation among the time slots span by a packet, with the final purpose of identifying the throughput-delay-reliability tradeoffs in single-hop scenarios. The temporal

correlation of interference and outage is further discussed in [11], where, additionally, a useful analysis has been developed to evaluate the mean interference at the origin and at the boundary of a finite network. A PPP-based model is also adopted in [12] to accurately compute the error probability in cellular networks exploiting multi-antenna systems for spatial multiplexing purposes. The accuracy of the PPP in describing the deployment of the base stations in cellular environment has been analyzed in [13], proving that the PPP can provide reliable results when used in conjunction with the deployment gain, a novel metric that quantifies the closeness of a real point set to a PPP. Furthermore, real base station locations available from publicly available databases have been adopted in [14] to realistically validate the accuracy of a PPP-based approach for modeling dense urban environments.

Even if the PPP represents a satisfactory model for large networks that enables the derivation of analytically tractable frameworks, some of its underlying assumptions may not hold in some practical scenarios where the number of nodes is low, non-isotropic conditions are present, or the number of nodes in disjoint areas cannot be considered independent. Hence, extended or alternative theoretical approaches have been proposed [15]–[20]. In particular, in [15], the authors consider a uniform distribution of the nodes over a disk, proving that, when the nodes may be arbitrarily close to one another, the results obtained by an unbounded path-loss model (UPM) may considerably deviate from those obtained by a more realistic bounded path-loss model (BPM). This behavior is confirmed by the analysis presented in [16], where the interference statistic and the transmission capacity are evaluated for the more general class of cluster PPPs under both the UPM and the BPM. A binomial point process is adopted in [17] to prove that the internode distance is described by a generalized beta distribution when the nodes are uniformly distributed (u.d.) inside a ball of arbitrary dimensions. An interesting proposal for overcoming the limitations of the PPP that holds in the high signal-to-interference (SIR) regime has been presented in [18]. More precisely, in [18], the asymptotic transmission capacity is evaluated modeling the success probability by two parameters that account for the spatial distribution of the interferers. In [19], a general class of spatial distributions, which includes the uniform distribution as a special case, is considered to derive the coverage probability in heterogeneous scenarios where each node may be characterized by its own antenna system. The interference distribution suffered by a randomly located source-destination link in a finite network with u.d. nodes is analyzed in [20], which represents one of the first studies that specifically considers the possibility of arbitrarily located receivers.

### *B. Motivation and Contribution*

Many of the above cited papers discuss the possible situations in which a PPP may become inaccurate, namely when networks with few nodes are analyzed [18], or when the assumption concerning the independence of the number of nodes in disjoint regions does not hold [17]. A further reason of possible inaccuracy for a PPP is the finite area occupied by the network, which leads to potential non-isotropic scenarios [17], where a given destination, from its own point of view, may not perceive the interferers as u.d. in angle. This aspect becomes very significant in multi-packet peer-to-peer networks, since each destination may be characterized by a specific coverage probability dependent on its position and on its antenna system. In the presence of sources u.d. over a disk, the distance of a destination from the center of the disk may be reasonably assumed as the most significant parameter to model the effect of the destination location if omnidirectional antennas are adopted. Differently, when the antenna pattern is shaped, the radial coordinate becomes no more sufficient to reliably characterize the result of a transmission attempt. In fact, in the presence of directional or smart antenna systems, the coverage probability is also determined by the angular coordinate of the destination and by the orientation of the receiving pattern. Thus, in a finite network, even if the sources are u.d. over a disk, the combination of a non-omnidirectional receiving pattern with a non-centered location of the destination may lead to highly non-isotropic interference distributions, whose evaluation requires a careful consideration of the angular domain beside the radial one.

The objective of this paper is to investigate this scenario, which, to the best of authors' knowledge, remains partly unexplored, since the few interference models considering a non-centered location of the destination focus on the omnidirectional antenna case [11], [20]. Accordingly, a mathematical framework is developed to evaluate the interference distribution, the coverage probability, and the transmission capacity in a multi-packet peer-to-peer network with u.d. sources, accounting for the actual location of each destination. The proposed model, which includes path-loss attenuation and fading effects, establishes the result of each communication according to the DOA statistic and the antenna processing technique. In particular, the analysis considers both interference mitigation, enabled by directional antennas, and interference suppression, enabled by adaptive arrays. The presented results, which are verified by Monte Carlo validations, explore the realistic situation that exists when a destination lies in a position different from the center of a finite network, and that requires to include the angular domain beside the radial one in order to reliably model the resulting non-isotropic interference scenario.

The paper is organized as follows. The geometry of the network is introduced in Section II. The spatial distributions of the nodes are derived in Section III. The interference analysis is developed in Section IV. Comparisons with existing models and asymptotic analysis are presented in Section V. The coverage probability is calculated in Section VI. The transmission capacity is evaluated in Section VII. The most relevant conclusions are summarized in Section VIII.

## II. Geometry Description

Consider a wireless network in which $L$ single-hop peer-to-peer communications are simultaneously active, thus involving $L$ sources and the corresponding $L$ destinations. Accordingly, each destination receives the power from its desired source and perceives the remaining $L-1$ active sources as interferers. The transmitting sources are characterized by an omnidirectional

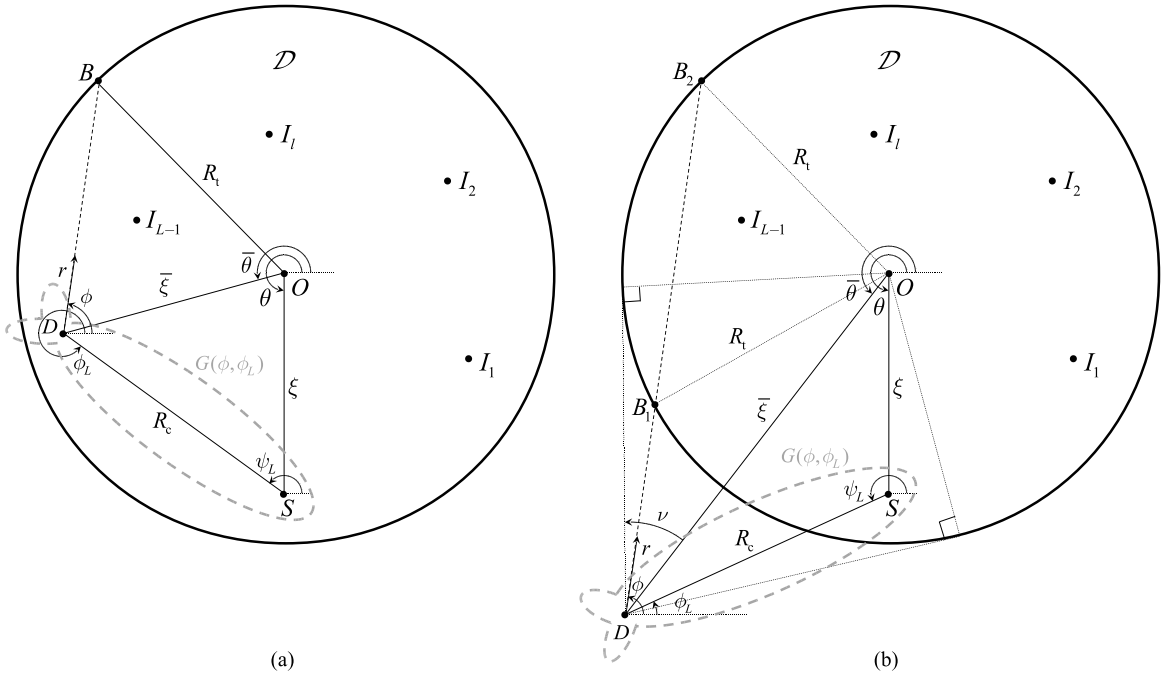


Fig. 1. Geometry of the scenario: (a) destination internal to the disk $\mathcal{D}$, (b) destination external to the disk $\mathcal{D}$.

antenna pattern having a power gain $G_{\text{tx}}$, while the destinations can use a generic receiving power pattern. The sources are u.d. over a disk $\mathcal{D}$ of center $O$ and radius $R_{\text{t}}$ (Fig. 1). With reference to a polar coordinate system with origin $O$, observe a generic communicating pair. This pair consists of a desired source in position $S = (\xi, \theta)$, where $\xi \in [0, R_{\text{t}}]$ and $\theta \in [0, 2\pi)$, and of its destination, which is u.d. over the circumference of center $S$ and radius equal to the source-destination distance $R_{\text{c}}$. Identify the observed pair by the index $L$ and use the indexes $1, \ldots, L-1$ to denote the other (interfering) pairs. The position of the destination with respect to $S$ can be denoted as $(R_{\text{c}}, \psi_L)$, where the angle $\psi_L$ from which the desired source communicates with its intended destination is u.d. over $[0, 2\pi)$. According to the resulting geometry, the position of the observed destination with respect to $O$ can be identified as $D = (\bar{\xi}, \bar{\theta})$, where:

$$\bar{\xi} = \sqrt{\xi^2 + R_{\text{c}}^2 + 2\xi R_{\text{c}} \cos(\psi_L - \theta)}, \tag{1}$$

and:

$$\bar{\theta} = \arg\left[\xi \cos\theta + R_{\text{c}} \cos\psi_L + i\,(\xi \sin\theta + R_{\text{c}} \sin\psi_L)\right], \tag{2}$$

with $i$ denoting the imaginary unit and $\arg(\cdot)$ denoting the argument function defined for $(\xi \cos\theta + R_{\text{c}} \cos\psi_L, \xi \sin\theta + R_{\text{c}} \sin\psi_L) \neq (0, 0)$. From now on, to avoid cumbersome notations, the result of any operation providing an angle, as for example (2), is interpreted modulo $2\pi$ within the interval $[0, 2\pi)$ [21]. Since $D$ is determined by the random values $\xi$, $\theta$, $\psi_L$ and by the distance $R_{\text{c}}$, the destination may lie inside $\mathcal{D}$ (Fig. 1(a)), or outside it (Fig. 1(b)). For both cases, consider a reference system integral with $D$, in which $\phi \in \Lambda_D$ denotes the azimuth angle, $r \in [\hat{d}_D(\phi), \tilde{d}_D(\phi)]$ denotes the distance, and where the interval $\Lambda_D$ and the endpoints $\hat{d}_D(\phi)$ and $\tilde{d}_D(\phi)$ depend on the position of the observed destination. These quantities can be derived by trigonometric considerations from Fig. 1(a) for the case $0 \leq \bar{\xi} \leq R_{\text{t}}$, and from Fig. 1(b) for the case $R_{\text{t}} < \bar{\xi} \leq R_{\text{t}} + R_{\text{c}}$. More precisely, $\Lambda_D$ is calculated as:

$$\Lambda_D = \begin{cases} [0, 2\pi) & 0 \leq \bar{\xi} \leq R_{\text{t}} \\ \left[\pi + \bar{\theta} - \nu, \pi + \bar{\theta} + \nu\right] & R_{\text{t}} < \bar{\xi} \leq R_{\text{t}} + R_{\text{c}} \end{cases} \tag{3}$$

where $\nu = \arcsin(R_{\text{t}}/\bar{\xi})$. The endpoint $\hat{d}_D(\phi)$ is zero for $0 \leq \bar{\xi} \leq R_{\text{t}}$, and is equal to the distance $\overline{DB}_1$ for $R_{\text{t}} < \bar{\xi} \leq R_{\text{t}} + R_{\text{c}}$ (Fig. 1(b)), while the endpoint $\tilde{d}_D(\phi)$ is equal to $\overline{DB}$ for $0 \leq \bar{\xi} \leq R_{\text{t}}$ (Fig. 1(a)), and to $\overline{DB}_2$ for $R_{\text{t}} < \bar{\xi} \leq R_{\text{t}} + R_{\text{c}}$ (Fig. 1(b)). Hence, after some algebra, one obtains:

$$\hat{d}_D(\phi) = \begin{cases} 0 & 0 \leq \bar{\xi} \leq R_{\text{t}} \\ \min[H_1(\phi), H_2(\phi)] & R_{\text{t}} < \bar{\xi} \leq R_{\text{t}} + R_{\text{c}} \end{cases} \tag{4}$$

$$\tilde{d}_D(\phi) = \begin{cases} H_2(\phi) & 0 \leq \bar{\xi} \leq R_{\text{t}} \\ \max[H_1(\phi), H_2(\phi)] & R_{\text{t}} < \bar{\xi} \leq R_{\text{t}} + R_{\text{c}} \end{cases} \tag{5}$$

where:

$$H_{1/2}(\phi) = \left| \sqrt{R_{\text{t}}^2 - \bar{\xi}^2 \sin^2(\phi - \bar{\theta})} \pm \bar{\xi} \cos(\phi - \bar{\theta}) \right|. \tag{6}$$

According to this reference system integral with $D$, the position $I_l$ of the $l$-th interferer ($l = 1, \ldots, L-1$) can be denoted as $(r_l, \phi_l)$, and that of the desired source as $(R_{\text{c}}, \phi_L)$. In particular, the angle $\phi_L$ from which the destination receives the transmission from its desired source is opposite to the angle $\psi_L$ from which the desired source sees the destination, thus:

$$\phi_L = \psi_L - \pi. \tag{7}$$

The transmissions of the desired source and of the interferers are received by the destination using an antenna power pattern $G(\phi, \phi_L)$, identified by the grey dashed lines in Fig. 1.

This geometric formulation is developed considering the quantities $R_\mathrm{t}$ and $R_\mathrm{c}$ as parameters, while $\xi, \theta, \psi_L, \bar{\xi}, \bar{\theta}, r_1, \ldots, r_{L-1}, \phi_1, \ldots, \phi_L$ are realizations of the random variables (r.v.s) $\Xi, \Theta, \Psi_L, \bar{\Xi}, \bar{\Theta}, R_1, \ldots, R_{L-1}, \Phi_1, \ldots, \Phi_L$, respectively. Concerning the choice of a constant $R_\mathrm{c}$ value, it is worth to observe that, since one of the purposes of the study is to analyze the impact of the destination location in multi-packet peer-to-peer scenarios, technical difficulties may arise considering u.d. sources and destinations. In this case, in fact, a rule should be established for associating a source and a destination already located in certain positions, with the additional drawback of potentially having very close pairs and very far ones. A situation that might partially hide the effect of the destination location with respect to the interferers. To avoid this event and to properly apply the concept of transmission capacity, the analysis has been developed considering a constant source-destination distance, which represents a common assumption [6], [8], [9], [11], [16], even when the directions are randomly selected [10], [18]. According to this network scenario, the theoretical analysis is carried out following four main steps: derivation of the spatial distributions (Section III), evaluation of the interference statistic and comparison with existing models (Sections IV and V, respectively), estimation of the coverage probability (Section VI), and calculation of the transmission capacity (Section VII).

## III. Spatial Distributions

Before starting to derive the spatial statistics, some relevant aspects may be outlined concerning the dependencies among the involved r.v.s and the peculiarities of the analyzed scenario.

First, one may identify a basic set of r.v.s that influence all the others. This set consists of the three independent r.v.s $\Xi$, $\Theta$, and $\Psi_L$. Since the position $S$ of the desired source is u.d. over $\mathcal{D}$ and is referred to the origin $O$, the joint probability density function (pdf) of $\Xi$ and $\Theta$ is:

$$f_{\Xi,\Theta}(\xi,\theta) = \frac{1}{\pi R_\mathrm{t}^2} \cdot \begin{cases} \xi & \xi \in [0, R_\mathrm{t}], \quad \theta \in [0, 2\pi) \\ 0 & \text{elsewhere} \end{cases} \tag{8}$$

Using (8), the marginal pdfs of $\Xi$ and $\Theta$ can be immediately obtained, respectively, as:

$$f_\Xi(\xi) = \int_0^{2\pi} f_{\Xi,\Theta}(\xi,\theta)\mathrm{d}\theta = \frac{2\xi}{R_\mathrm{t}^2} \cdot [u_1(\xi) - u_0(\xi - R_\mathrm{t})], \tag{9a}$$

$$f_\Theta(\theta) = \int_0^{R_\mathrm{t}} f_{\Xi,\Theta}(\xi,\theta)\mathrm{d}\xi = f_\mathrm{UC}(\theta), \tag{9b}$$

where $u_j(x)$ is the unit step function with the value in $x = 0$ defined by the parameter $j \in \{0, 1\}$, that is, $u_j(x) = 0$ if $x < 0$, $u_j(x) = 1$ if $x > 0$, $u_j(0) = j$. Besides, in (9b), the function:

$$f_\mathrm{UC}(x) = \frac{1}{2\pi} \cdot [u_1(x) - u_1(x - 2\pi)], \tag{10}$$

denotes the circularly uniform (c.u.) distribution [22]. Recalling that the destination location is u.d. over a circumference of radius $R_\mathrm{c}$, one can infer that $\Psi_L$ is c.u.. Hence, since $\Psi_L$ and $\Phi_L$ are related by (7) and the c.u. distribution is invariant under rotation [21], also $\Phi_L$ is c.u., thus:

$$f_{\Phi_L}(\phi_L) = f_\mathrm{UC}(\phi_L). \tag{11}$$

Remembering that the position of each source over the disk $\mathcal{D}$ remains u.d. (in area) regardless of the point of observation ($O$, $S$, or $D$), and that the position of each interferer is independent of the position of the others, the joint pdf of $R_l$ and $\Phi_l$ given $\bar{\Xi}$ and $\bar{\Theta}$ for $l = 1, \ldots, L-1$ is:

$$f_{R_l,\Phi_l|\bar{\Xi},\bar{\Theta}}(r_l,\phi_l|\bar{\xi},\bar{\theta}) = \frac{1}{\pi R_\mathrm{t}^2} \cdot \begin{cases} r_l & r_l \in [\hat{d}_D(\phi_l), \tilde{d}_D(\phi_l)], \quad \phi_l \in \Lambda_D \\ 0 & \text{elsewhere} \end{cases} \tag{12}$$

In particular, (12) identifies the joint pdf of the radial and angular coordinates, seen by a destination lying in position $D = (\bar{\xi}, \bar{\theta})$, of an interferer $l$ u.d. over $\mathcal{D}$. Differently from the case in which $D$ coincides with $O$, the r.v. $\Phi_l$ is no more circularly u.d., and, moreover, $R_l$ and $\Phi_l$ are dependent, because, according to (12), $\phi_l$ influences the range $[\hat{d}_D(\phi_l), \tilde{d}_D(\phi_l)]$ in which $r_l$ is generated. Furthermore, since (12) is a conditional pdf given $\bar{\Xi}$ and $\bar{\Theta}$, the r.v.s $R_l$ and $\Phi_l$ (for $l = 1, \ldots, L-1$) depend, by (1) and (2), on the basic r.v.s $\Xi$, $\Theta$, and $\Psi_L$.

Now that the basic set of r.v.s has been identified, some fundamental propositions may be formulated to make some introductory considerations concerning the perception of the source locations from the point of view of a non-centered destination.

*Proposition 1:* The distribution of the angular position of each interferer seen by $D$, that is, the marginal pdf of $\Phi_l$ given $\bar{\Xi}$ and $\bar{\Theta}$ for $l = 1, \ldots, L-1$, is given by:

$$f_{\Phi_l|\bar{\Xi},\bar{\Theta}}(\phi_l|\bar{\xi},\bar{\theta}) = \frac{1}{2\pi R_\mathrm{t}^2} \cdot \begin{cases} \varsigma_D(\phi_l) & \phi_l \in \Lambda_D \\ 0 & \text{elsewhere} \end{cases} \tag{13}$$

where:

$$\varsigma_D(x) = \begin{cases} R_\mathrm{t}^2 + \bar{\xi}^2 \cos[2(x-\bar{\theta})] - \zeta_D(x) & 0 \le \bar{\xi} \le R_\mathrm{t} \\ -2\zeta_D(x) & R_\mathrm{t} < \bar{\xi} \le R_\mathrm{t} + R_\mathrm{c} \end{cases} \tag{14}$$

and:

$$\zeta_D(x) = 2\bar{\xi}\cos(x - \bar{\theta})\sqrt{R_\mathrm{t}^2 - \bar{\xi}^2 \sin^2(x - \bar{\theta})}. \tag{15}$$

*Proof:* Use (4)-(6) in (12) and integrate on all $R_l$ values. □

*Proposition 2:* The distribution of the radial position of each interferer seen by $D$, that is, the marginal pdf of $R_l$ given $\bar{\Xi}$ and $\bar{\Theta}$ for $l = 1, \ldots, L-1$, is given by:

$$f_{R_l|\bar{\Xi}}(r_l|\bar{\xi}) = \frac{2}{R_\mathrm{t}^2} \cdot \begin{cases} r_l\, u_1(R_\mathrm{t} - \bar{\xi}) & 0 < r_l \le |R_\mathrm{t} - \bar{\xi}| \\ \dfrac{r_l}{\pi} \arccos\left(\dfrac{\bar{\xi}^2 + r_l^2 - R_\mathrm{t}^2}{2\bar{\xi} r_l}\right) & |R_\mathrm{t} - \bar{\xi}| < r_l \le R_\mathrm{t} + \bar{\xi} \\ 0 & \text{elsewhere} \end{cases} \tag{16}$$

*Proof:* Use (4)-(6) in (12) and then integrate on the values of $\Phi_l$ belonging to the intersection between the interval $\Lambda_D$ and the solution of the inequality $\hat{d}_D(\phi_l) \le r_l \le \tilde{d}_D(\phi_l)$. □

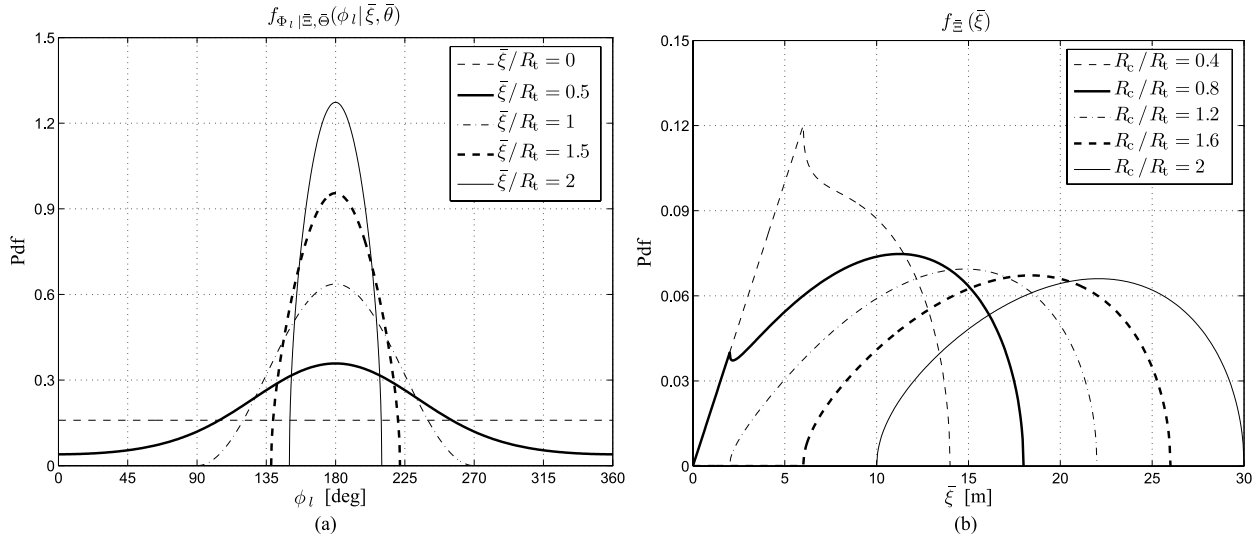


Fig. 2. Spatial statistics obtained for $R_t = 10$ m: (a) marginal pdf of $\Phi_l$ given $\bar{\Xi}$ and $\bar{\Theta}$ for $\bar{\theta} = 0$ and different values of $\bar{\xi}/R_t$, (b) pdf of $\bar{\Xi}$ for different values of $R_c/R_t$.

Observe that the marginal pdf in (16) is not influenced by the angle between the observed destination and the origin $O$, thus $f_{R_l|\bar{\Xi},\bar{\Theta}}(r_l|\bar{\xi},\bar{\theta}) = f_{R_l|\bar{\Xi}}(r_l|\bar{\xi})$. Besides, as expected, except for the case $\bar{\xi} = 0$, the product between the two marginals in (13) and (16) does not provide the joint pdf in (12), since $\Phi_l$ and $R_l$ are dependent for $l = 1, ...L-1$.

According to the geometry in Fig. 1, the r.v.s $\bar{\Theta}$ and $\bar{\Xi}$ can be viewed as the argument and the magnitude, respectively, of the vector sum $(\xi\cos\theta, \xi\sin\theta) + (R_c\cos\psi_L, R_c\sin\psi_L)$. Since the r.v.s involved in this sum derive from a uniform distribution on a disk and a c.u. distribution, $\bar{\Theta}$ and $\bar{\Xi}$ are independent and $\bar{\Theta}$ is circularly u.d. [21], thus:

$$f_{\bar{\Theta}}(\bar{\theta}) = f_{\mathrm{UC}}(\bar{\theta}). \tag{17}$$

By consequence, the joint pdf of $\bar{\Theta}$ and $\bar{\Xi}$ can be directly calculated as the product between $f_{\bar{\Theta}}(\bar{\theta})$ and the marginal pdf of $\bar{\Xi}$, for which the following proposition holds.

*Proposition 3:* The distribution of the radial position of the destination, that is, the marginal pdf of $\bar{\Xi}$, is given by:

$$f_{\bar{\Xi}}(\bar{\xi}) = \frac{2}{R_t^2} \cdot \begin{cases} \bar{\xi}\, u_1(R_t - R_c) & 0 \le \bar{\xi} \le |R_t - R_c| \\ \dfrac{\bar{\xi}}{\pi}\arccos\left(\dfrac{R_c^2 + \bar{\xi}^2 - R_t^2}{2R_c\bar{\xi}}\right) & |R_t - R_c| < \bar{\xi} \le R_t + R_c \\ 0 & \text{elsewhere} \end{cases} \tag{18}$$

*Proof:* See Appendix A. □

### A. Results

To clarify the results obtained in this section, Fig. 2 reports, for $R_t = 10$ m, the pdf $f_{\Phi_l|\bar{\Xi},\bar{\Theta}}(\phi_l|\bar{\xi},\bar{\theta})$ of the angle from which the destination perceives an interferer (Fig. 2(a)), and the pdf $f_{\bar{\Xi}}(\bar{\xi})$ of the distance between the destination and the origin $O$ (Fig. 2(b)). Fig. 2(a) shows that a destination lying at a distance $\bar{\xi}$ from $O$ perceives the interferer as circularly u.d. just for $\bar{\xi} = 0$, while the conditional pdf of $\Phi_l$ gets higher in a set of directions that becomes narrower as $\bar{\xi}$ increases. Concerning the distance $\bar{\xi}$, Fig. 2(b) shows that, if $R_c \le R_t$, $f_{\bar{\Xi}}(\bar{\xi})$ increases linearly for $\bar{\xi} \le R_t - R_c$ and then behaves nonlinearly for $R_t - R_c < \bar{\xi} \le R_t + R_c$. With reference to Fig. 2(a), it may be interesting to outline an analogy with the results obtained in [23], which do not concern the destination displacement with respect to the center of the network, but the power azimuth spectrum perceived by a receiver from a transmitter lying at the center of a disk of u.d. scatterers. This analogy reveals that a peripheral position of the destination introduces a directionality similar to that introduced by a channel with a low angular spread. This phenomenon may remain relevant even in the presence of an omnidirectional reception, since the angular coordinate $\Phi_l$ of the interferer is in general not circularly u.d. with respect to $D$.

The result in (16) may intuitively suggest that a destination lying at the periphery of the network should receive a lower interference, because the interferers are statistically more distant. However, this argument directly holds if omnidirectional patterns are adopted. Otherwise, the response might be not so immediate. In fact, a destination adopting a shaped pattern and lying in a position displaced from $O$ indeed perceives the interferers as more distant, but may be forced to steer the main lobe of its pattern just towards the directions of interference, since its desired source lies in the same region $\mathcal{D}$ where the interferers lie. This aspect requires a deeper investigation of the relationship between destination location and receiving antenna gain, which represents, together with the impact of the propagation channel, the aim of the next section.

## IV. Interference Analysis

### A. Antenna and Channel Models

The receiving power pattern $G(\phi, \phi_L)$ is modeled considering an end-fire array of $N$ elements, which generates a pattern

that can be expressed in closed-form as [24]:

$$G(\phi,\phi_L)=\begin{cases}\left|\dfrac{\sin\{N\pi\,[\cos(\phi-\phi_L)-1]/4\}}{N\sin\{\pi\,[\cos(\phi-\phi_L)-1]/4\}}\right|^2 & \phi\neq\phi_L\\ 1 & \phi=\phi_L\end{cases} \tag{19}$$

The omnidirectional pattern, which is determined by a unity gain in the entire angular domain, that is, $G(\phi,\phi_L)=1$ for $\phi\in[0,2\pi)$, can be obtained directly from (19) by imposing $N=1$. Even if the proposed framework can operate using any shape for $G(\phi,\phi_L)$, the end-fire array has been preferred because it is capable to generate realistic patterns that can be represented by the well-established expression in (19), thus allowing the reproducibility of the presented results.

The propagation environment is modeled accounting for multipath-fading and path-loss attenuation, considering multipath-fading effects in space-time domain. Concerning the spatial domain, when a signal is transmitted by a source lying at an angle $\phi$ with respect to the destination, its DOA at the destination is the realization $\phi'\in[0,2\pi)$ of a r.v. $\Phi'$, since the signal is spread across the angular domain. Among the large number of available DOA statistics, the truncated Laplacian is the most widely used [25], thanks to its experimentally assessed adherence to the real channel behavior [26]. Accordingly, the pdf of $\Phi'$ given $\Phi$ is selected as [26]:

$$f_{\Phi'|\Phi}(\phi'|\phi)=\frac{K_{\mathrm{L}}}{\sqrt{2}\,\sigma_\phi}e^{-\frac{\sqrt{2}}{\sigma_\phi}|\phi'-\phi|}\cdot u_1\left(\frac{\pi}{2}-|\phi'-\phi|\right), \tag{20}$$

where $K_{\mathrm{L}}$ is a normalization constant and $\sigma_\phi$ is the angular spread. The combined effect of antenna system and spatial channel model can be modeled by the equivalent pattern [27]:

$$\mathcal{G}(\phi,\phi_L)=\int_0^{2\pi}G(\phi',\phi_L)f_{\Phi'|\Phi}(\phi'|\phi)\mathrm{d}\phi', \tag{21}$$

in which the equivalent gain in a direction $\phi$ is obtained by averaging the antenna pattern according to the pdf of the DOA referred to that direction. It is interesting to observe that the concept of equivalent pattern adopted in [27] is strictly related to the Q-parameter used in [7], since both quantities model the combined effect of power gain pattern and DOA statistic. The main difference between the two definitions is that the Q-parameter in [7] includes the path-loss exponent and hence implicitly assumes an UPM, while the equivalent pattern in [27], not including the path-loss exponent, may be used under both the UPM and the BPM.

Concerning the multipath-fading effects in the time domain, the power fluctuation due to the mobility between the observed destination and the generic $l$-th source (desired or interfering) can be modeled by a r.v. $Q_l$, having as pdf a gamma density with unit mean [11]:

$$f_{Q_l}(q_l)=\frac{m^m}{\Gamma(m)}q_l^{m-1}e^{-mq_l}u_0(q_l), \tag{22}$$

where $m(\geq 1/2)$ is the Nakagami parameter and $\Gamma(\cdot)$ is the gamma function.

The BPM is adopted to model path-loss attenuation [15]. Accordingly, the power $p_l$ received by the observed destination from the $l$-th interferer ($l=1,\ldots,L-1$) may be expressed as:

$$p_l=\frac{P_{\mathrm{tx}}K_{\mathrm{c}}G_{\mathrm{tx}}\mathcal{G}(\phi_l,\phi_L)}{1+r_l^\alpha}q_l=t_lq_l, \tag{23}$$

where $P_{\mathrm{tx}}$ is the transmission power (assumed equal for all sources), $K_{\mathrm{c}}$ is a constant accounting for the wavelength of the carrier signal, $\alpha$ is the path-loss exponent, and:

$$t_l=\frac{K_{\mathrm{tx}}\mathcal{G}(\phi_l,\phi_L)}{1+r_l^\alpha}, \tag{24}$$

with $K_{\mathrm{tx}}=P_{\mathrm{tx}}K_{\mathrm{c}}G_{\mathrm{tx}}$. Therefore, the received power $p_l$ in (23) is expressed as the product between $t_l$, which accounts for the equivalent pattern, the path-loss model, and the spatial distribution of the interferers, and $q_l$, which accounts for the fading statistic. The BPM is selected for its capability to overcome some limitations of the classic UPM, which is suitable to analyze scenarios in which the interferers are distant from the destination, but may provide unrealistic results when a destination and an interferer can be arbitrarily close to one another [15]. For completeness, the constant $K_{\mathrm{tx}}$ will be maintained in the subsequent calculations, but, without loss of generality, it will be assumed of unity value when numerical results will be presented.

### *B. Interference Statistics*

For $l=1,\ldots,L-1$, the r.v. $T_l$ defined by (24) depends on the r.v. $\Phi_L$ and on the r.v.s $R_l$ and $\Phi_l$, whose joint pdf given $\bar{\Xi}$ and $\bar{\Theta}$ is defined in (12). Therefore, one may evaluate the pdf of $T_l$ given $\Phi_L$, $\bar{\Xi}$, and $\bar{\Theta}$, namely given the direction of the desired source and the destination location. Observing the pdfs in (11), (17), and (18), one can infer that these three latter variables are independent of each other. Thus, their joint pdf can be expressed as the product:

$$f_{\mathbf{V}}(\mathbf{v})=f_{\Phi_L}(\phi_L)f_{\bar{\Xi}}(\bar{\xi})f_{\bar{\Theta}}(\bar{\theta}), \tag{25}$$

where the random vector $\mathbf{V}=(\Phi_L,\bar{\Xi},\bar{\Theta})$ and its corresponding realization $\mathbf{v}=(\phi_L,\bar{\xi},\bar{\theta})$ are introduced to simplify the notation in the subsequent calculations. From now on, $\mathbf{v}$ will be referred to as the spatial context of the destination. This definition allows one to formulate the following proposition.

*Proposition 4:* The distribution of the interference power received by $D$ from the generic fixed $l$-th interferer, that is, the pdf of $T_l$ given $\mathbf{V}$ for $l=1,\ldots,L-1$, is given by:

$$f_{T_l|\mathbf{V}}(t_l|\mathbf{v})=\frac{K_{\mathrm{tx}}}{\alpha\pi\,R_{\mathrm{t}}^2}\int_{\Delta_{\mathbf{v},\Phi_l}}\frac{\mathcal{G}(\phi_l,\phi_L)}{t_l^2}\times\left[\frac{K_{\mathrm{tx}}\mathcal{G}(\phi_l,\phi_L)}{t_l}-1\right]^{\frac{2}{\alpha}-1}\mathrm{d}\phi_l, \tag{26}$$

where $\Delta_{\mathbf{v},\Phi_l}=\{\phi_l:(t_l,\phi_l)\in\Delta_{\mathbf{v}}\}$ and:

$$\Delta_{\mathbf{v}}=\left\{(t_l,\phi_l):\frac{K_{\mathrm{tx}}\mathcal{G}(\phi_l,\phi_L)}{\tilde{d}_D^\alpha(\phi_l)+1}\leq t_l\leq\frac{K_{\mathrm{tx}}\mathcal{G}(\phi_l,\phi_L)}{\hat{d}_D^\alpha(\phi_l)+1},\phi_l\in\Lambda_D\right\}. \tag{27}$$

*Proof:* See Appendix B. □

This proposition enables to derive the power received by the observed destination from the $l$-th mobile interferer. In fact, using (22), (23), and (26), the conditional pdf of the r.v. $P_l = T_l Q_l$ can be evaluated by applying the relationship for the product between r.v.s [28], thus obtaining:

$$f_{P_l|\mathbf{V}}(p_l|\mathbf{v}) = \frac{m^m}{\Gamma(m)} \int_0^{+\infty} q_l^{m-2} e^{-mq_l} f_{T_l|\mathbf{V}}\left(\frac{p_l}{q_l}\middle|\mathbf{v}\right) \mathrm{d}q_l. \quad (28)$$

for $l = 1, \ldots, L-1$. In general, $f_{T_l|\mathbf{V}}(t_l|\mathbf{v})$, and hence $f_{P_l|\mathbf{V}}(p_l|\mathbf{v})$, cannot rely on closed-form expressions, since, according to (27), the subdomain $\Delta_{\mathbf{v},\Phi_l}$ used in (26) is implicitly defined by the equivalent pattern $\mathcal{G}(\phi_l, \phi_L)$, which is a not invertible function of $\phi_l$. Therefore, to reduce the further computational burden necessary to evaluate the statistic of the total interference power due to the $L-1$ interferers, some approximations are adopted. These approximations are introduced considering the capabilities of the receiving antenna system of the destination. In particular, two processing techniques are analyzed: interference mitigation (IM), in which just beam steering is enabled, and interference suppression (IS), in which both beam and null steering are enabled.

The IM case is already modeled by the directional end-fire radiation pattern in (19), which, by (21), provides the equivalent pattern that accounts for the pdf of the DOA. The IS case, instead, is modeled recalling that an array of $N$ elements provides $N-1$ degrees of freedom (dofs). In a peer-to-peer scenario with $L$ communicating pairs, each destination has a unique desired source, thus one dof is used to steer the main lobe towards the desired direction and $N-2$ dofs remain available for interference suppression [27]. Since adaptive arrays aim to maximize the SIR at the destination, it is reasonable to assume that these $N-2$ dofs are used to suppress the strongest interferers among the $L-1$ ones [7]. Even if the secondary lobes of the receiving pattern synthesized by a beamforming algorithm may be influenced by the directions in which the nulls must be placed, the equivalent pattern obtained by (19) and (21) for the IM case is maintained as the reference pattern also for the IS case. Otherwise, an almost untractable number of situations should be considered and the possible reproduction of the results would become awkward. According to these considerations, one may identify the number of dofs available for interference suppression in the IM and IS cases as:

$$N_\mathrm{e} = \begin{cases} 0 & \text{using IM} \\ \max(0, N-2) & \text{using IS} \end{cases} \quad (29)$$

The omnidirectional antenna case ($N = 1$), which in practice does not provide IM or IS capabilities, has been however included in (29) for mathematical purposes.

The above considerations enable the formulation of the following proposition.

*Proposition 5:* The distribution of the total interference received by $D$, that is, the pdf of $P_\mathrm{I} = \sum_{l=1}^{L-1} P_l$ given $\mathbf{V}$, may be estimated by (30), as shown at the bottom of the page, where $\beta(\cdot,\cdot)$ is the beta function and:

$$F_{P_l|\mathbf{V}}(p_l|\mathbf{v}) = \int_0^{p_l} f_{P_l|\mathbf{V}}(p_l'|\mathbf{v}) \mathrm{d}p_l', \quad (31a)$$

$$\bar{F}_{P_l|\mathbf{V}}(p_l|\mathbf{v}) = 1 - F_{P_l|\mathbf{V}}(p_l|\mathbf{v}), \quad (31b)$$

represent, respectively, the cumulative distribution function (cdf) and the complementary cdf (ccdf) of $P_l$ given $\mathbf{V}$.

*Proof:* See Appendix C. □

Concerning the approximation in (30), one may remember that the total interference is usually approximated accounting only for the strongest interferer [11]. However, this approach may be too coarse if the path-loss exponent becomes close to 2 [29]. Therefore, (30) has been developed considering also the second strongest interferer when two or more undesired sources remain not suppressed (case $L > N_\mathrm{e} + 2$) in order to reliably account for the case $\alpha = 2$. A further advantage of (30) concerns its ability to directly provide the conditional pdf of $P_\mathrm{I}$ for a given $L$ without requiring the intermediate evaluation of the cases $l < L$, which instead would be necessary if the classic approach based the $(L-1)$-fold convolution of (28) would be adopted. This is particularly useful to reduce the computational complexity for large $L$ values, since, regardless of the number of interferers, (30) requires at most one integral instead of $L-1$.

### C. Results

To provide a view of the impact of some of the introduced quantities on the statistic of the interference, Figs. 3 and 4 show, for $R_\mathrm{t} = 10$ m and $\alpha = 3$ in the IM case, the pdf $f_{P_\mathrm{I}|\mathbf{V}}(p_\mathrm{I}; L|\mathbf{v})$ in different scenarios. In particular, Fig. 3(a) refers to the omnidirectional antenna case when a unique interferer is present ($L = 2$). In this case, the values of the destination's angular coordinate $\bar{\theta}$ and of the desired direction $\phi_L$ have no impact on the results, since the antenna gain is identical in all directions. Hence, $f_{P_\mathrm{I}|\mathbf{V}}(p_\mathrm{I}; L|\mathbf{v})$ depends only on the destination's radial coordinate $\bar{\xi}$, whose increase leads to a lower probability of receiving a high interference power. This confirms that, in terms of perceived interference, the periphery of the network represents an advantageous position for a destination equipped with an omnidirectional antenna. When a directional pattern is adopted, instead, the scenario becomes more complex (Fig. 3(b)). More precisely, with respect to the case $N = 1$, the use of a directional pattern ensures a decrease of the received interference for all values of $\phi_L$

$$f_{P_\mathrm{I}|\mathbf{V}}(p_\mathrm{I}; L|\mathbf{v}) \cong \begin{cases} (N_\mathrm{e}+1)\, \bar{F}_{P_l|\mathbf{V}}^{N_\mathrm{e}}(p_\mathrm{I}|\mathbf{v}) f_{P_l|\mathbf{V}}(p_\mathrm{I}|\mathbf{v}) & L = N_\mathrm{e}+2 \\ \displaystyle\int_0^{+\infty} \frac{F_{P_l|\mathbf{V}}^{L-N_\mathrm{e}-3}(p_l|\mathbf{v}) f_{P_l|\mathbf{V}}(p_l|\mathbf{v}) \bar{F}_{P_l|\mathbf{V}}^{N_\mathrm{e}}(p_\mathrm{I}-p_l|\mathbf{v}) f_{P_l|\mathbf{V}}(p_\mathrm{I}-p_l|\mathbf{v})}{\beta(L-N_\mathrm{e}-2, N_\mathrm{e}+2)} \mathrm{d}p_l & L > N_\mathrm{e}+2 \end{cases} \quad (30)$$

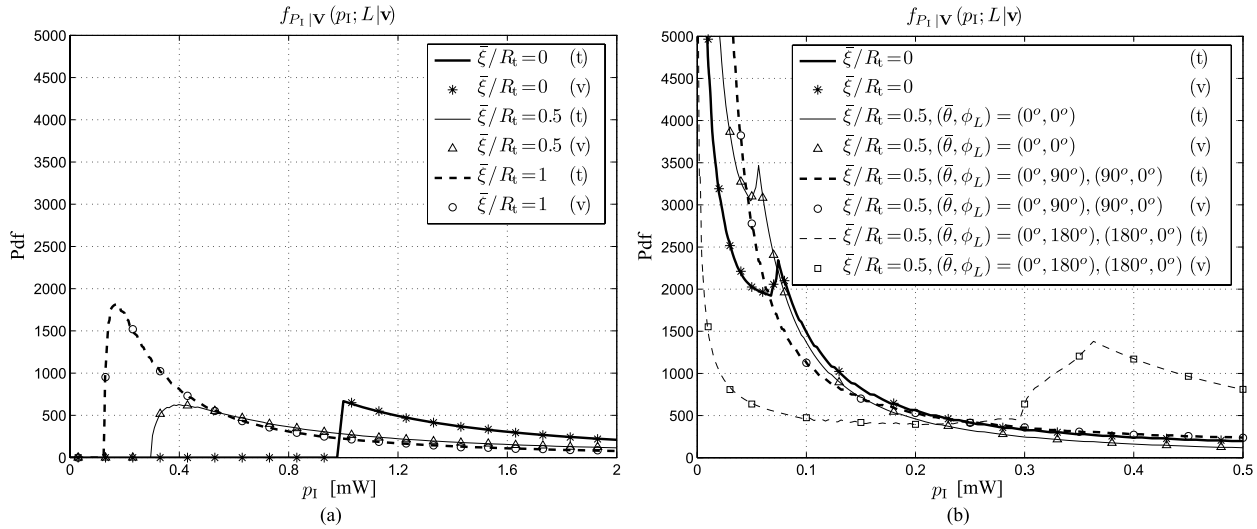


Fig. 3. Pdf of the conditional interference power for $L=2$ in absence of multipath-fading: (a) $N=1$ and different values of $\bar{\xi}/R_{\rm t}$, (b) $N=4$ with IM and different values of $\bar{\xi}/R_{\rm t}$, $\bar{\theta}$, and $\phi_L$ (t: theory, v: Monte Carlo validation).

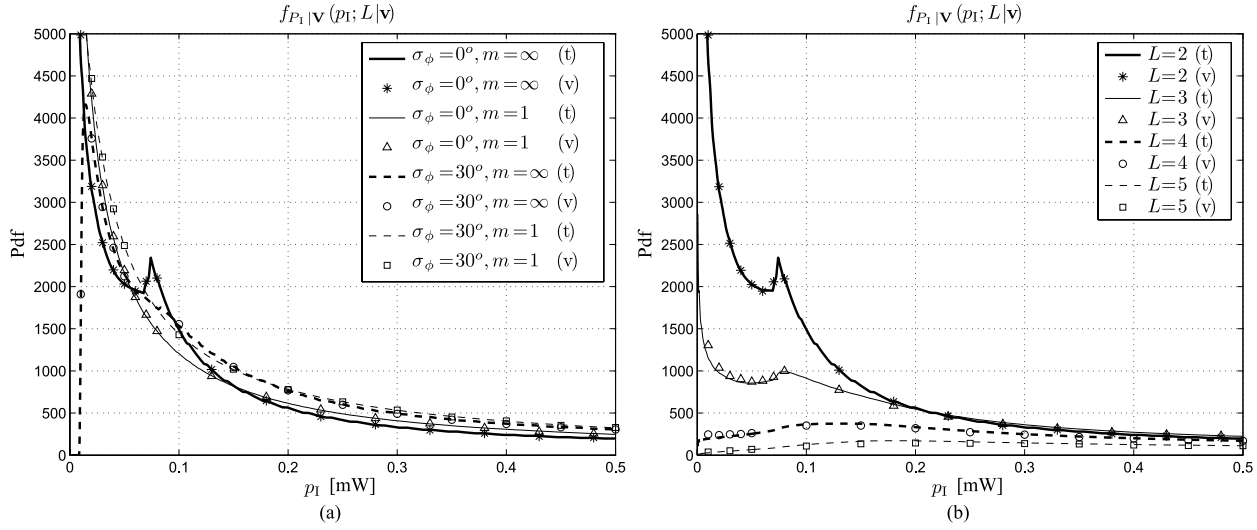


Fig. 4. Pdf of the conditional interference power for $\bar{\xi}=0$ and $N=4$ with IM: (a) $L=2$ and different values of $\sigma_\phi$ and $m$, (b) absence of multipath-fading and different values of $L$ (t: theory, v: Monte Carlo validation).

when $\bar{\xi}=0$, since $f_{P_{\rm I}|\mathbf{V}}(p_{\rm I}; L|\mathbf{v})$ remains not dependent on $\bar{\theta}$ and $\phi_L$. On the other hand, when $\bar{\xi}/R_{\rm t}=0.5$ and the main lobe of the receiving pattern is not steered towards the inner of $\mathcal{D}$ (cases $(\bar{\theta},\phi_L)=(0°,90°)$ and $(\bar{\theta},\phi_L)=(90°,0°)$), the probability of receiving a high interference is low. Otherwise, when this main lobe is steered exactly towards the inner of $\mathcal{D}$ (cases $(\bar{\theta},\phi_L)=(0°,180°)$ and $(\bar{\theta},\phi_L)=(180°,0°)$), the probability of receiving a high interference increases. Therefore, even if, adopting a directional pattern, a destination not close to the center of the network usually experiences a lower interference, there are some specific cases in which this interference may be significant.

This reveals that the angles $\bar{\theta}$ and $\phi_L$ may have a crucial effect on the perceived interference, which may remain relevant also when compared to that due to multipath-fading (Fig. 4(a)) and to that due to the presence of a further interferer (case $L=3$ in Fig. 4(b)). This suggests that a reliable modeling of the destination location including the angular domain beside the radial one may be fundamental for an accurate analysis of a multi-packet peer-to-peer network in which shaped antenna patterns are adopted. As a final comment concerning Figs. 3 and 4, one may notice that the figures also report, for each theoretically derived curve (represented by a line), the corresponding Monte Carlo validation (represented by markers). The direct comparison between theory and validation reveals that (30) provides a really satisfactory approximation for the pdf of $P_{\rm I}$.

## V. Comparison and Asymptotic Analysis

### A. Comparison With Existing Models

Further considerations regarding the proposed interference analysis may be formulated by looking at the frameworks developed in [11] and [20], which model network

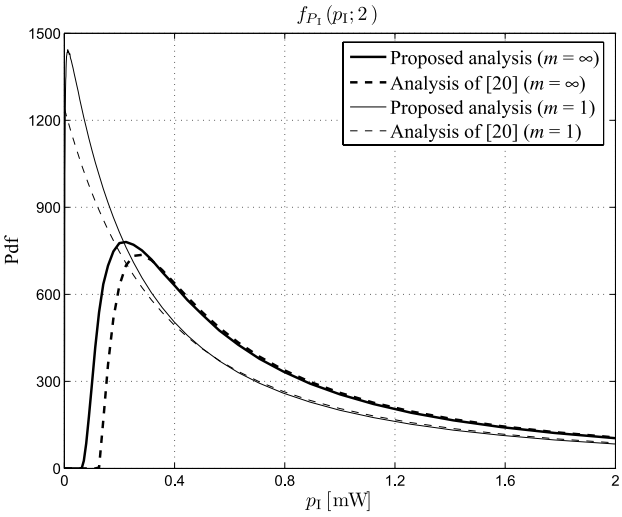


Fig. 5. Pdf of the interference power obtained using the proposed analysis and the analysis of [20].

scenarios characterized by non-centered destinations using omnidirectional antennas. As outlined in Subsection IV-C, in the case $N = 1$ the pdf of the interference depends only on the displacement with respect to the center of the network and not on the angles $\bar{\theta}$ and $\phi_L$, thus in this subsection the spatial context will be described by the sole radial coordinate $\bar{\xi}$.

A first comparison is carried out adopting the pdf of the interference power evaluated in [20, eqs.(3)–(5)], which is derived using an UPM when both the sources and the destinations are u.d. inside $\mathcal{D}$. Recalling that [20] considers a unique interferer and provides an unconditional pdf, a proper comparison with the proposed model requires that $f_{P_\mathrm{I}|\bar{\Xi}}(p_\mathrm{I}; 2|\bar{\xi})$ be averaged over all possible displacements in order to evaluate the corresponding unconditional pdf:

$$f_{P_\mathrm{I}}(p_\mathrm{I}; 2) = \int_0^{R_\mathrm{t}+R_\mathrm{c}} f_{P_\mathrm{I}|\bar{\Xi}}(p_\mathrm{I}; 2|\bar{\xi}) f_{\bar{\Xi}}(\bar{\xi}) \mathrm{d}\bar{\xi}, \tag{32}$$

where $f_{\bar{\Xi}}(\bar{\xi})$ is given by (18). The curves obtained from the two models for $R_\mathrm{t} = 10$ m, $R_\mathrm{c} = 4$ m, and $\alpha = 3$ are reported in Fig. 5. These curves reveal that the two theories provide results in good agreement. The slight difference, more evident for low $p_\mathrm{I}$ values, may be explained remembering that the model in [20] considers the UPM and a destination always internal to $\mathcal{D}$, while the proposed model adopts the BPM and considers the possibility of having a destination external to $\mathcal{D}$. Thus, one may reasonably expect to obtain a slightly more interfered scenario using the analysis of [20] and a slightly less interfered scenario using the proposed model.

Two further comparisons are carried out considering the framework presented in [11], which enables to derive the mean interference at the center and at the boundary of $\mathcal{D}$ when the sources are distributed according to a PPP. In particular, for the here proposed model, the mean conditional interference received by a destination characterized by a displacement $\bar{\xi}$ in the presence of $L$ active sources, that is, $L-1$ interferers, may be immediately obtained as:

$$\mathrm{E}[P_\mathrm{I}|\bar{\Xi}] = \int_0^{+\infty} p_\mathrm{I} f_{P_\mathrm{I}|\bar{\Xi}}(p_\mathrm{I}; L|\bar{\xi}) \mathrm{d}p_\mathrm{I}. \tag{33}$$

In order to obtain a fair comparison between the presented theory and the analysis of [11], the parameters adopted in the two models must be properly matched. More precisely, the mean interference for a PPP may be derived from the analysis of [11, Sec. 3] and [29, Sec. 3.2.1] by recalling that a BPM has been adopted and by setting the intensity $\lambda$ of the interfering sources of the PPP equal to $(L-1)/(\pi R_\mathrm{t}^2)$. This enables the evaluation of the mean interference for a PPP at the center ($\bar{\xi} = 0$) and at the boundary ($\bar{\xi} = R_\mathrm{t}$) of $\mathcal{D}$ as:

$$\mathrm{E}^{\mathrm{PPP}}[P_\mathrm{I}|\bar{\Xi}] = \frac{L-1}{\pi R_\mathrm{t}^2}\left(2-\frac{\bar{\xi}}{R_\mathrm{t}}\right)\int_{-\pi/2}^{\pi/2}\int_0^{h(\bar{\xi},\vartheta)} \frac{r'}{1+r'^{\alpha}} \mathrm{d}r' \mathrm{d}\vartheta, \tag{34}$$

where $h(\bar{\xi},\vartheta) = (R_\mathrm{t}+\bar{\xi})\cos(\vartheta\bar{\xi}/R_\mathrm{t})$. Observe that (33) holds for any $\bar{\xi}$ value lying between 0 and $R_\mathrm{t}+R_\mathrm{c}$, while (34) holds just for $\bar{\xi} = 0$ and $\bar{\xi} = R_\mathrm{t}$ (a unique expression for the two values has been formulated for compactness reasons). Fig. 6(a) reports, for $R_\mathrm{t} = 10$ m, $R_\mathrm{c} = 4$ m, and $\alpha = 3$, the mean conditional interference obtained by (33) for $0 \le \bar{\xi} \le R_\mathrm{t}+R_\mathrm{c}$ (lines) and by (34) for $\bar{\xi} = 0, R_\mathrm{t}$ (filled markers), considering different $L$ values. In addition to the significant matching between the two compared approaches for $\bar{\xi} = 0$ and $\bar{\xi} = R_\mathrm{t}$, it is interesting to observe that, until the destination becomes very close to the boundary of $\mathcal{D}$, the mean interference decreases very slowly moving from the center to the periphery of the network. A more specific investigation, focused on the mean interference at the center and the boundary of $\mathcal{D}$ (Fig. 6(b)), confirms that the two models are in good agreement. In particular, for $\bar{\xi} = 0$, the results remain coincident, while, for $\bar{\xi} = R_\mathrm{t}$, some differences may appear when the radius of the topology and the path-loss exponent become low.

### *B. Asymptotic Analysis*

An analytical characterization of the mean interference in the presence of directional antennas may be obtained adopting an infinitesimal beamwidth model [19], in which the desired source is received with a unity gain and an interferer is received with an average equivalent gain:

$$\bar{\mathcal{G}} = \frac{1}{4\pi^2}\int_0^{2\pi}\int_0^{2\pi} \mathcal{G}(\phi,\phi_L)\mathrm{d}\phi\,\mathrm{d}\phi_L. \tag{35}$$

This model has the significant advantage of providing some useful insights on the interference statistic simultaneously enabling the derivation of closed-form expressions. In particular, this subsection investigates the asymptotic behavior of $\mathrm{E}[P_\mathrm{I}|\bar{\Xi}]$ for large $R_\mathrm{t}$ values, focusing on the center and the boundary of $\mathcal{D}$, where the following proposition holds.

*Proposition 6:* For $\alpha > 2$ in the presence of an infinitesimal beamwidth model of gain $\bar{\mathcal{G}}$, the mean interference at the center of $\mathcal{D}$ is given by:

$$\mathrm{E}[P_\mathrm{I}^\mathrm{c}] = \frac{2K_{\mathrm{tx}}\bar{\mathcal{G}}(L-1)}{\alpha R_\mathrm{t}^2}\left[\frac{\pi}{\sin(2\pi/\alpha)} + \mathcal{F}(2,\alpha,R_\mathrm{t})\right], \tag{36}$$

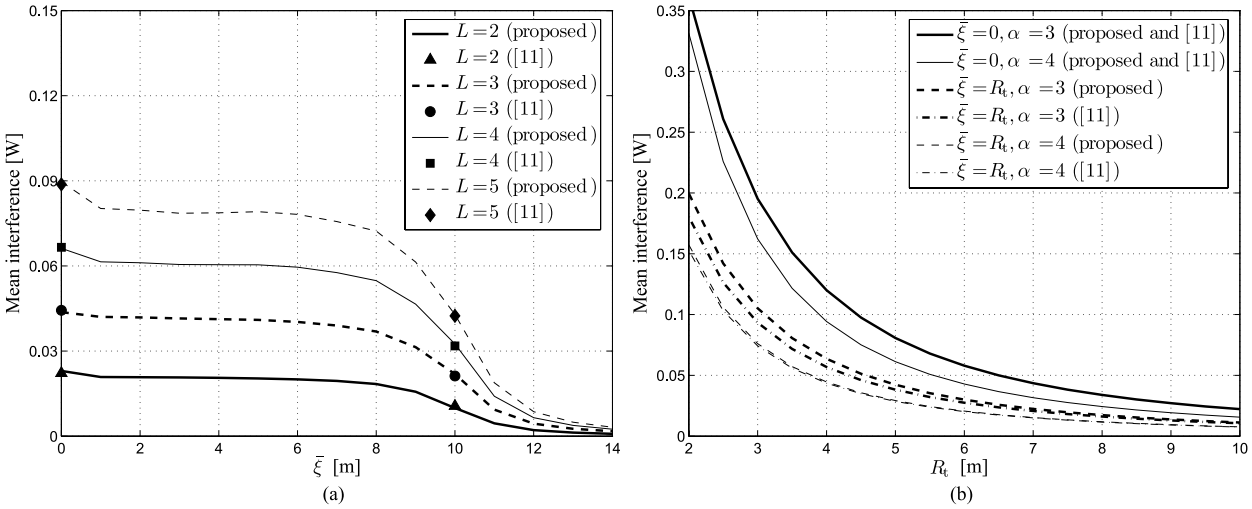


Fig. 6. Conditional mean interference power obtained using the proposed analysis and the analysis of [11]: (a) different $L$ values as a function of $\bar{\xi}$ for $\alpha = 3$, (b) different $\alpha$ values as a function of $R_{\mathrm{t}}$ at the center and at the boundary of $\mathcal{D}$ for $L = 2$.

while the mean interference at the boundary of $\mathcal{D}$ is upper bounded by:

$$\mathrm{E}[P_{\mathrm{I}}^{\mathrm{b}}] \lesssim \frac{K_{\mathrm{tx}}\bar{\mathcal{G}}(L-1)}{\alpha R_{\mathrm{t}}^2}\left[\frac{\pi}{\sin(2\pi/\alpha)} + \mathcal{F}(2,\alpha,2R_{\mathrm{t}}) - \frac{2}{\pi}\mathcal{F}(3,\alpha,2R_{\mathrm{t}})\right], \tag{37}$$

where "$\lesssim$" denotes an upper bound with asymptotic equality [11], and $\mathcal{F}(k,\alpha,x)$, reported in (38) at the bottom of this page, is defined for $k = 2, 3$ with ${}_2F_1(\cdot,\cdot;\cdot;\cdot)$ representing the hypergeometric function [30].

*Proof:* See Appendix D. □

Proposition 6 shows that the mean interference approaches zero when $R_{\mathrm{t}}$ becomes large, regardless of the destination location. This behavior is expected, since an increase of $R_{\mathrm{t}}$ for a given number of interferers $L-1$ leads to a reduction of the interferers' density in $\mathcal{D}$. A confirmation is given by Fig. 7, which reports $\mathrm{E}[P_{\mathrm{I}}^{\mathrm{c}}]$, $\mathrm{E}[P_{\mathrm{I}}^{\mathrm{b}}]$, and the upper bound in (37) for $L = 5$. The curves show the monotonic increase of the mean interference with the average receiving gain and reveal that the estimated bound is very close to $\mathrm{E}[P_{\mathrm{I}}^{\mathrm{b}}]$.

As a final comment concerning (36) and (37), one may observe that $\mathcal{F}(k,\alpha,x)$ in (38), as shown at the bottom of the page, approaches zero when $x \to +\infty$. Thus, the following corollary may be formulated.

*Corollary 1:* When $R_{\mathrm{t}} \to +\infty$, $\mathrm{E}[P_{\mathrm{I}}^{\mathrm{b}}] \lesssim \frac{1}{2}\mathrm{E}[P_{\mathrm{I}}^{\mathrm{c}}]$.

A similar result has been derived in [11, Cor. 4] for a homogeneous PPP with a uniform mobility model. This seems to suggest that, regardless that the nodes' distribution relies on a constant density of interferers or on a constant number of interferers, the mean interference at the boundary of a finite network asymptotically approaches half of the mean interference at its center.

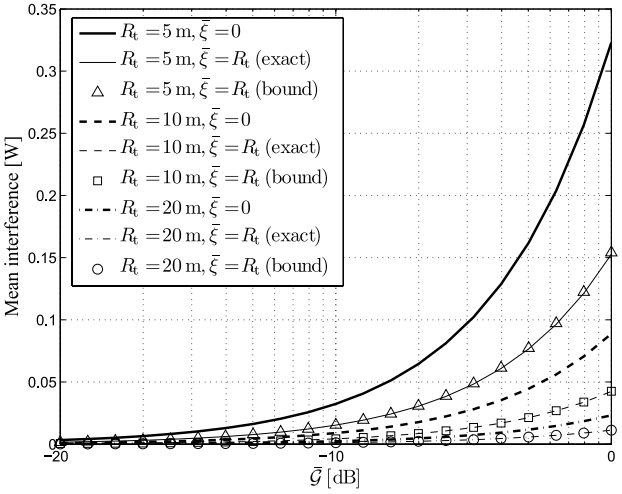


Fig. 7. Mean interference at the center and at the boundary of $\mathcal{D}$ as a function of the average gain for different $R_{\mathrm{t}}$ values.

## VI. Coverage Probability

Once the interference statistic is evaluated, the next step of the analysis consists in the estimation of the coverage probability. Remembering that the observed pair is identified by the index $L$ and that the source-destination distance is equal to $R_{\mathrm{c}}$, the power received by the destination from the desired source in the absence of mobility may be

$$\mathcal{F}(k,\alpha,x) = \frac{1}{x^{k-2}} \cdot \begin{cases} \log(1+x^{\alpha}) & k=\alpha=3 \\ \dfrac{\pi(k-2)}{\sin(3\pi/\alpha)} - \dfrac{\alpha(1+x^{\alpha})^{\frac{k}{\alpha}-1}}{\alpha-k}\,{}_2F_1\left(1-\dfrac{k}{\alpha}, 1-\dfrac{k}{\alpha}; 2-\dfrac{k}{\alpha}; \dfrac{1}{1+x^{\alpha}}\right) & \text{otherwise} \end{cases} \tag{38}$$

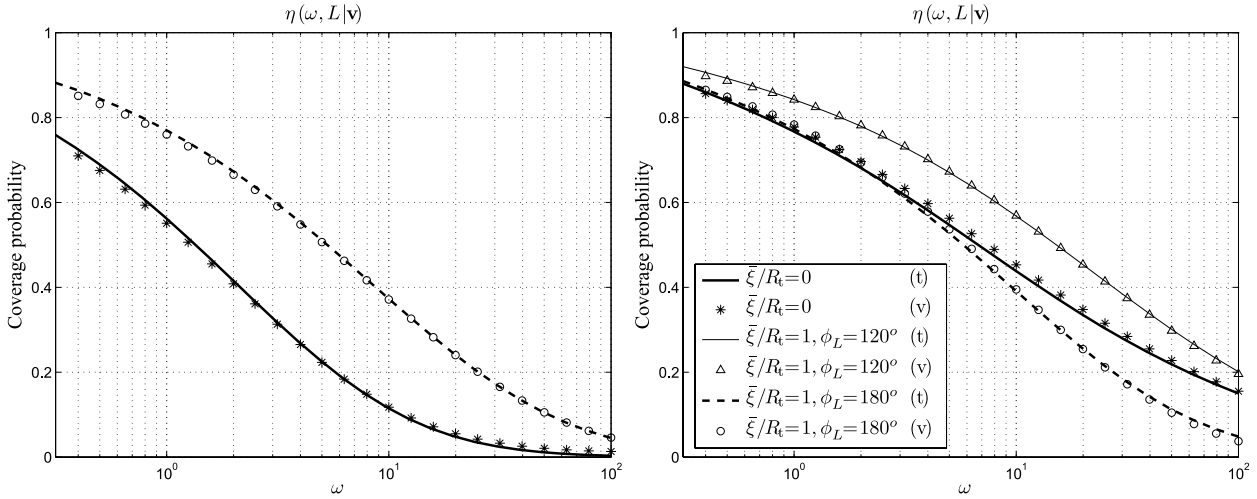


Fig. 8. Coverage probability at the center ($\bar{\xi}/R_t = 0$) and at the boundary ($\bar{\xi}/R_t = 1$) of $\mathcal{D}$: (a) $N = 1$, (b) $N = 4$ with IM and different values of $\phi_L$ (t: theory, v: Monte Carlo validation).

calculated as:

$$\bar{t}_L = \frac{K_{tx}\mathcal{G}(\phi_L, \phi_L)}{1 + R_c^{\alpha}}, \tag{39}$$

where, according to (19) and (21), the receiving equivalent power gain $\mathcal{G}(\phi_L, \phi_L)$ in the desired direction is equal to one when $\sigma_\phi = 0°$, and is lower than one when $\sigma_\phi > 0°$. Hence, recalling (22) and the rule for the scaling of r.v.s [28], the pdf of the r.v. $P_L = \bar{t}_L Q_L$, which identifies the desired signal power, may be represented by a gamma density of mean $\bar{t}_L$, that is:

$$f_{P_L}(p_L) = \left(\frac{m}{\bar{t}_L}\right)^m \frac{p_L^{m-1}}{\Gamma(m)} e^{-m\frac{p_L}{\bar{t}_L}} u_0(p_L). \tag{40}$$

The corresponding cdf may be evaluated from (40) as:

$$F_{P_L}(p_L) = \frac{1}{\Gamma(m)} \gamma\left(m, m\,\frac{p_L}{\bar{t}_L}\right), \tag{41}$$

where $\gamma(\cdot,\cdot)$ is the lower incomplete gamma function [30]. One can now investigate the SIR $\rho = p_L/p_I$ of the destination. In particular, the cdf of the r.v. SIR $= P_L/P_I$ given $\mathbf{V}$ may be derived using (41) and applying the rule for the ratio between r.v.s [28], thus obtaining:

$$F_{\mathrm{SIR}|\mathbf{V}}(\rho; L|\mathbf{v}) = \frac{1}{\Gamma(m)} \int_0^{+\infty} f_{P_I|\mathbf{V}}(p_I; L|\mathbf{v}) \times \gamma\left(m, m\frac{\rho p_I}{\bar{t}_L}\right) \mathrm{d}\, p_I. \tag{42}$$

The success or the failure of the communication attempt of the observed pair may be established adopting a reception threshold $\omega$ on the SIR [2], [16], [19], in order to model the characteristics of the communication system (packet length, channel coding rate, modulation scheme, packet error rate). According to the antenna processing technique adopted by the destination (IM or IS), when $L < N_e + 2$, no interference is present and hence the coverage probability is assumed equal to one (the noise effects are considered negligible at the involved distances). Otherwise, when $L \geq N_e + 2$, the coverage probability may be evaluated from the ccdf of (42). Therefore, for $L \in \mathbb{N}^+$, the conditional coverage probability may be calculated as:

$$\eta(\omega, L|\mathbf{v}) = \begin{cases} 1 & L < N_e + 2 \\ \bar{F}_{\mathrm{SIR}|\mathbf{V}}(\omega; L|\mathbf{v}) & L \geq N_e + 2 \end{cases} \tag{43}$$

This quantity represents the probability of success for a destination lying in a position $D = (\bar{\xi}, \bar{\theta})$ and having its desired source in the direction $\phi_L$, when other $L - 1$ transmissions are in progress and a communication system characterized by a reception threshold $\omega$ is adopted.

### A. Results

The result achieved in this subsection is used to obtain Fig. 8, which reports the coverage probability for a destination lying at the center and at the boundary of $\mathcal{D}$ for $R_c/R_t = 0.4$, $\bar{\theta} = 0°$, $\alpha = 3$, $L = 3$, $\sigma_\phi = 0°$, and $m = 1$. In particular, the values in Fig. 8(a), which are obtained considering an omnidirectional receiving pattern, confirm the intuition that a destination lying at the periphery of $\mathcal{D}$ is characterized by a larger coverage probability as compared to a destination placed at the center of $\mathcal{D}$. Instead, in the presence of a directional reception, Fig. 8(b) shows that, in some situations, the boundary of the network may not represent an advantageous position. In fact, taking as reference the case $\bar{\xi} = 0$, one may observe that, when the main lobe is steered towards the center of $\mathcal{D}$ (case $\phi_L = 180°$), the coverage probability decreases for a communication system requiring a threshold larger than 2, while, when $\phi_L = 120°$, $\eta(\omega, L|\mathbf{v})$ increases for all $\omega$ values. Therefore, the angular domain may have an impact even stronger than that of the radial one on the result of a transmission when the combined effect of node location and non-omnidirectional reception is taken into account.

## VII. Transmission Capacity

The developed analysis may be usefully employed to evaluate the performance of a multi-packet peer-to-peer network

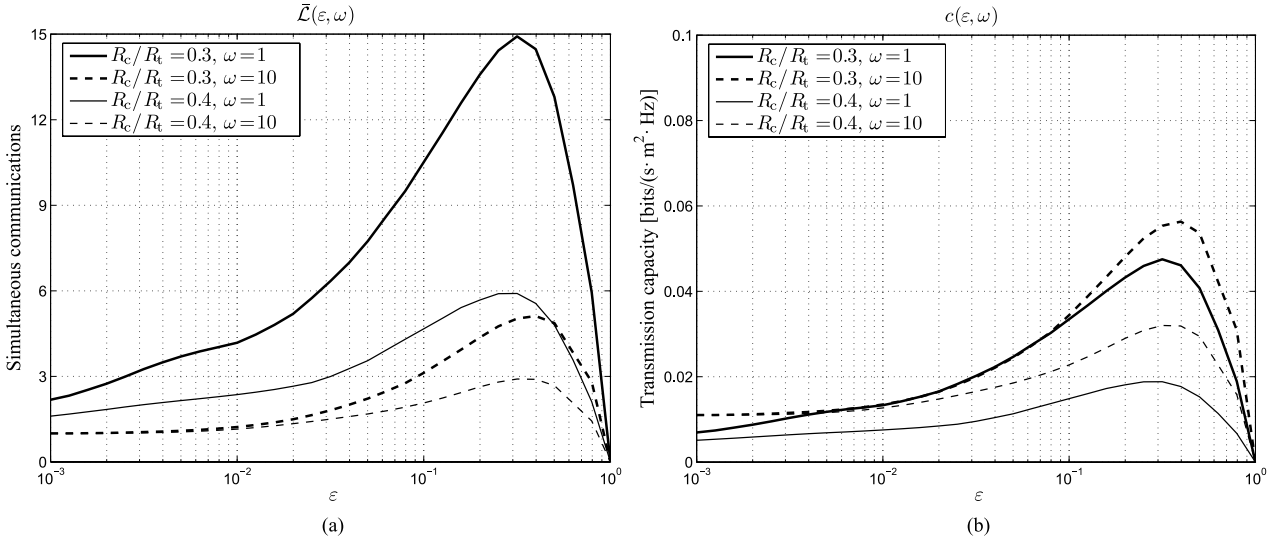


Fig. 9. Performance as a function of the outage threshold for $\alpha = 3$ and $N = 4$ with IM: (a) simultaneous communications, (b) transmission capacity.

by using the concept of transmission capacity, which may be slightly reformulated with respect to its original definition in [5]. To this purpose, one may initially define the quantity:

$$\mathcal{L}(\varepsilon,\omega,\mathbf{v}) = (1-\varepsilon)\ \sup_{L\in\mathbb{N}^+}\{L : \eta(\omega, L|\mathbf{v}) \geq 1-\varepsilon\}, \qquad (44)$$

which identifies, from the point of view of a destination characterized by a reception threshold $\omega$ and a spatial context $\mathbf{v}$, the maximum number of transmissions that may be sustained in $\mathcal{D}$ when a threshold $\varepsilon \in (0,1)$ on the outage probability is imposed. To account for all possible locations and antenna pattern orientations of the destination, (44) is averaged over all possible spatial contexts identified by the pdf of $\mathbf{V}$ in (25), thus obtaining:

$$\bar{\mathcal{L}}(\varepsilon,\omega) = \int_{\mathbb{D}} \mathcal{L}(\varepsilon,\omega,\mathbf{v})\, f_{\mathbf{V}}(\mathbf{v})\mathrm{d}\mathbf{v}, \qquad (45)$$

where $\mathbb{D} = [0, 2\pi)\times[0, R_t+R_c]\times[0, 2\pi)$ is the domain of the spatial context of the destination and $\mathrm{d}\mathbf{v} = \mathrm{d}\phi_L \mathrm{d}\bar{\xi}\mathrm{d}\bar{\theta}$. Finally, using the average number of successful (not in outage) simultaneous communications in (45), the transmission capacity can be evaluated as [6]:

$$c(\varepsilon,\omega) = \log_2(1+\omega)\frac{\bar{\mathcal{L}}(\varepsilon,\omega)}{\pi R_t^2}, \qquad (46)$$

by considering the Shannon bound in order to infer the limiting network performance [10]. Observe that the here considered formulation of the transmission capacity agrees with that presented in [5] and [6], even if, in [5] and [6], the definition of $c(\varepsilon,\omega)$ is formulated according to the adopted Poisson-based approach from the density of transmitting sources, while, in this study, (46) is formulated for a given spatial context from the number of transmitting sources. More precisely, $c(\varepsilon,\omega)$, which, as in [5] and [6], is evaluated in bits/(s · m$^2$ · Hz), represents the product between the spectral efficiency of a successful transmission and the maximum density of successful transmissions averaged over all the possible spatial contexts. The choice of relying, in (44), on the number of transmissions, and not on their density, enables to account for the non-isotropic characteristics of the analyzed scenario due to presence of different spatial contexts in which a destination may have to operate.

### A. Results

The numerical results presented in this section are derived in absence of multipath-fading for $R_t = 10$ m. Fig. 9 reports the number of simultaneous communications (Fig. 9(a)) and the transmission capacity (Fig. 9(b)) as a function of the outage threshold for $\alpha = 3$, $N = 4$, and different values of $\omega$ and $R_c/R_t$ in the presence of IM. As expected, for a given SIR threshold $\omega$, a lower source-destination distance leads to a larger number of communications and to a higher transmission capacity. On the other hand, for a given $R_c/R_t$ value and a given $\varepsilon$ value, a lower SIR threshold provides a larger number of communications, but does not ensure a higher transmission capacity. In particular, one may compare, in Fig. 9(b), the two curves corresponding to $\omega = 1$ (0 dB), and $\omega = 10$ (10 dB) for $R_c/R_t = 0.3$. This comparison reveals that, for some outage thresholds, a communication system characterized by a lower SIR threshold may enable a so high number of simultaneous communications that it may become able to compensate the gap due its lower spectral efficiency, thus leading to a transmission capacity almost equal to that provided by a communication system characterized by a higher SIR threshold. Therefore, in general, for a given outage constraint, a system adopted to maximize the number of served users does not necessarily maximize also the transmission capacity.

Fig. 10 shows the transmission capacity for $R_c/R_t = 0.4$. In particular, Fig. 10(a) reports $c(\varepsilon,\omega)$ as a function of the outage threshold for $\alpha = 3$, $\omega = 1$, and different receiving antenna systems. Instead, Fig. 10(b) reports $c(\varepsilon,\omega)$ as a function of the SIR threshold for $\varepsilon = 0.01$, $N = 8$, and different $\alpha$ values in the presence of IS. Fig. 10(a) confirms the expected significant increase of transmission

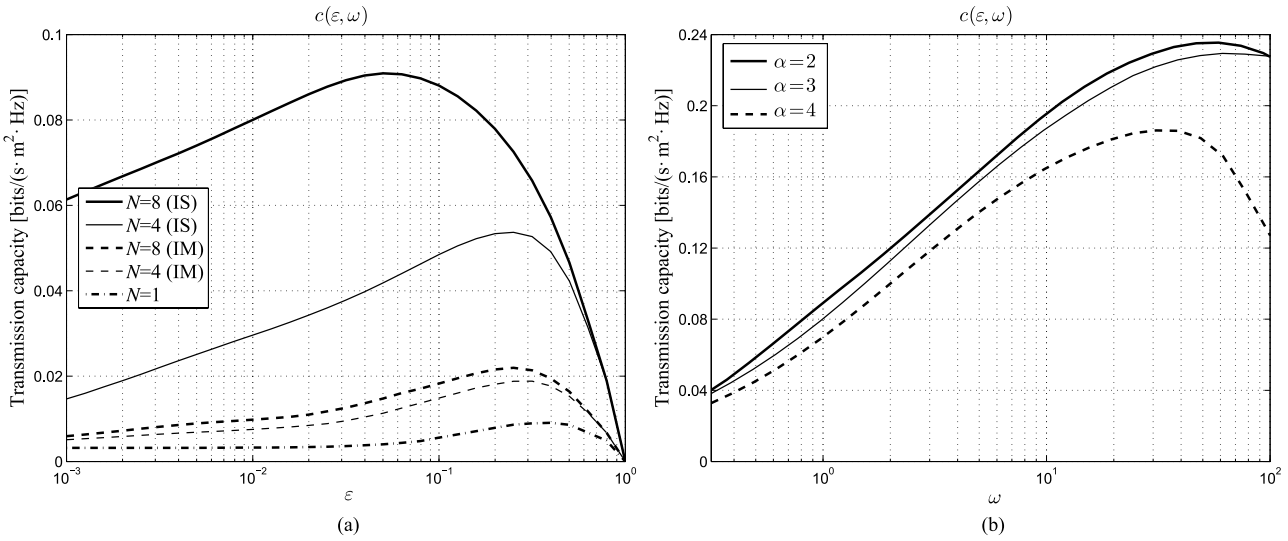


Fig. 10. Transmission capacity for $R_c/R_t = 0.4$: (a) as a function of the outage threshold for $\alpha = 3$ and $\omega = 1$ considering different values of $N$ and different antenna processing techniques, (b) as a function of the SIR threshold for $\varepsilon = 0.01$ and $N = 8$ with IS considering different values of $\alpha$.

capacity that may be achieved in the presence of antenna systems providing IS capabilities. To this purpose, one may observe that the introduction of the sole directionality in reception already provides considerable benefits in terms of transmission capacity, as it may be noticed by comparing the cases $N = 1$ and $N = 4$ with IM. However, in the IM case, a further increase of the number of antenna elements until $N = 8$ leads indeed to further improvements, but not to a proportional increase of $c(\varepsilon, \omega)$ with respect to the scenario with $N = 4$. This improvement is in fact just due to the more effective spatial filtering enabled by a receiving pattern with a reduced side-lobe level and a narrower main lobe. Differently, the availability of a receiving system with IS capabilities enables a better exploitation of the further dofs available when $N$ increases from 4 to 8, since these dofs are directly used to suppress the undesired sources. In the case $N = 1$, more than one communication is allowed only when $\varepsilon$ is larger than 0.1, since the interference is not suppressed or mitigated. Besides, when $N = 1$, the achievement of a $c(\varepsilon, \omega)$ value slightly larger than that corresponding to the single communication case is enabled by a weak outage constraint combined with the presence of destinations close to the boundary of the disk $\mathcal{D}$. Another aspect that is put into evidence by Fig. 10(a) concerns the $\varepsilon$ value that provides the maximum transmission capacity. This value becomes lower as the receiving antenna system becomes more sophisticated, that is, as the number of antenna elements increases and/or the interference is more effectively reduced. By consequence, more sophisticated antenna systems may support more stringent outage requirements when the objective is to maximize the transmission capacity. A further advantage provided by an antenna system adopting IS is represented by its capability of supporting communication systems characterized by a high SIR threshold (Fig. 10(b)), which allows one to achieve considerable $c(\varepsilon, \omega)$ values (observe that the ordinate axes of Fig. 10(a) and Fig. 10(b) have different scales). When the objective is to select the $\omega$ value that maximizes the transmission capacity, also the path-loss exponent should be taken into account, since Fig. 10(b) suggests that a lower value of $\alpha$ may lead to a better performance because of the lower attenuation suffered by the desired signal.

The results presented in this section have investigated the transmission capacity achievable in a finite peer-to-peer network with multi-packet capabilities. In particular, to obtain concise measures, thus enabling the discussion of the influence of each considered parameter on the performance, a suitable operation of averaging has been carried out in (45). Precisely because of this operation the importance of the spatial context might seem less evident. More precisely, while the inclusion of the angular domain has been proved to be fundamental for a reliable modeling of the interference received by a given destination as well as for establishing its coverage probability, it may seem unclear if this inclusion remains relevant when applied to evaluate not the single-node performance, but the performance of the overall network. In fact, the averaging operation might introduce a sort of compensation between destinations characterized by advantageous and disadvantageous spatial contexts, thus providing a network transmission capacity very close to that achievable assuming an isotropic model. To investigate this issue, the transmission capacity derived using the proposed analysis has been compared to that derived from two isotropic models, in which the destination is placed at the center of the disk $\mathcal{D}$. The first isotropic model is obtained by considering u.d. sources, while the second one is obtained considering the sources distributed according to a homogeneous PPP of intensity $\lambda = (L-1)/(\pi R_t^2)$. The derivation of the transmission capacity for this second case is described in Appendix E.

The result of the comparison between isotropic and non-isotropic models is reported in Fig. 11 for $R_c/R_t = 0.4$, $\alpha = 3$, $\omega = 1$, and different antenna systems. The figure shows that, for a given $\varepsilon$ value, the $c(\varepsilon, \omega)$ values obtained from the non-isotropic model are higher than or equal to

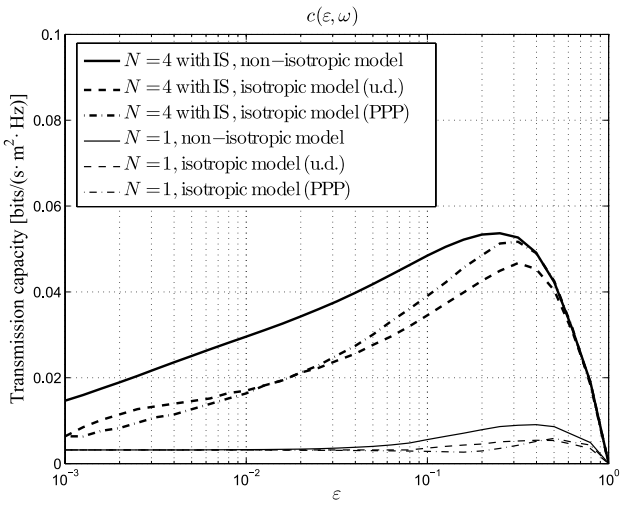


Fig. 11. Comparison, for $R_c/R_t = 0.4$, $\alpha = 3$, $\omega = 1$, and different antenna systems, between the transmission capacity obtained from the proposed non-isotropic analysis, and that obtained from two isotropic models: one adopting u.d. sources and another one assuming the sources distributed according to a homogeneous PPP.

those derived by the two isotropic models. This is due to the influence of the peripheral destinations, which may sometimes experience a low coverage probability but, for most of the spatial contexts, are characterized by $\eta(\omega, L|\mathbf{v})$ values higher than those achievable by the destinations close to the center of the network. Therefore, the coverage probability of each peripheral destination has a not negligible impact on the transmission capacity of the overall network. This reveals that, in a finite network, the spatial context, and hence the angular domain, may result relevant also when aggregate or average performance figures have to be considered.

## VIII. Conclusions

A theoretical model for including the angular domain beside the radial one in the analysis of a finite multi-packet peer-to-peer network has been developed. The interference statistic, the coverage probability, and the transmission capacity have been evaluated in non-isotropic scenarios, in which each destination may operate in a specific spatial context.

The results have shown that, when omnidirectional antennas are adopted, the periphery of the network represents an advantageous location in terms of received interference and coverage probability. This feature often holds also when shaped receiving patterns are adopted, but, in this case, the destination's angular position and the direction of the main lobe of its radiation pattern become fundamental for a reliable estimation of the actual result of a transmission attempt. The numerical values derived by the proposed theory have also revealed that a communication system characterized by a low spectral efficiency usually leads to a low transmission capacity, but, if the number of simultaneous communications that it enables is very high, its transmission capacity may match that of a communication system with a higher spectral efficiency. Besides, the further improvements that may be obtained by increasing the number of elements of the destination's antenna system seem better exploited in the presence of adaptive arrays, which enable the suppression of the interferers.

In summary, the presented theory has shown that, when the angular domain is included in the analysis of a finite multi-packet peer-to-peer scenario, the resulting non-isotropic view of the network leads to a non-isotropic coverage probability, and, in turn, to a larger transmission capacity with respect to the isotropic case. This relaxation of the isotropy assumption may be helpful to derive a more exhaustive estimation of the network behavior, since a given performance metric may be realistically evaluated considering the actual spatial context in which each source-destination pair has to communicate.

## Appendix A
## Proof of Proposition 3

Since $\Theta$ and $\Psi_L$ are circularly u.d., also the r.v. $\Upsilon = \Psi_L - \Theta$ is circularly u.d. [21]. Hence, the two independent r.v.s $\Xi$, having pdf in (9a), and $\Upsilon$, having pdf $f_\Upsilon(\upsilon) = f_{UC}(\upsilon)$, have joint pdf:

$$f_{\Xi,\Upsilon}(\xi,\upsilon) = \frac{1}{\pi R_t^2} \cdot \begin{cases} \xi & \xi \in [0, R_t], \quad \upsilon \in [0, 2\pi) \\ 0 & \text{elsewhere} \end{cases} \tag{47}$$

The method of transformation of r.v.s by inverse mapping [31], may be used to obtain the joint pdf $f_{\Xi,\bar{\Xi}}(\xi,\bar{\xi})$ from the joint pdf $f_{\Xi,\Upsilon}(\xi,\upsilon)$ using the transformation $(\Xi,\Upsilon) \to (\Xi,\bar{\Xi})$. The direct transformation from $\Upsilon$ to $\bar{\Xi}$ is defined recalling (1) with $\psi_L - \theta = \upsilon$, which leads to:

$$\bar{\xi} = \sqrt{\xi^2 + R_c^2 + 2\,\xi R_c \cos\upsilon}, \tag{48}$$

while the inverse transformation from $\bar{\Xi}$ to $\Upsilon$ is evaluated by inverting (48) on the two disjoint subsets $Z_1 = [0, R_t] \times [0, \pi)$ and $Z_2 = [0, R_t] \times [\pi, 2\pi)$ in order to maintain a one-to-one mapping between the support of $f_{\Xi,\Upsilon}(\xi,\upsilon)$ and that of $f_{\Xi,\bar{\Xi}}(\xi,\bar{\xi})$. The above operations yield:

$$\upsilon_k(\xi,\bar{\xi}) = \arccos\left(\frac{\bar{\xi}^2 - \xi^2 - R_c^2}{2\xi R_c}\right) + (k-1)\pi, \tag{49}$$

for $k = 1, 2$. According to these transformations, the joint pdf of $\Xi$ and $\bar{\Xi}$ can be derived as [31]:

$$f_{\Xi,\bar{\Xi}}(\xi,\bar{\xi}) = \sum_{k=1}^{2} |J_k| \cdot f_{\Xi,\Upsilon}[\xi, \upsilon_k(\xi,\bar{\xi})], \tag{50}$$

where:

$$J_k = \begin{vmatrix} \dfrac{\partial\xi}{\partial\xi} & \dfrac{\partial\xi}{\partial\bar{\xi}} \\ \dfrac{\partial\upsilon_k}{\partial\xi} & \dfrac{\partial\upsilon_k}{\partial\bar{\xi}} \end{vmatrix}, \tag{51}$$

is the determinant of the Jacobian associated to the transformation corresponding to the subset $Z_k$. Thus, using (47) and (49) in (50) and (51), after some manipulations one obtains:

$$f_{\Xi,\bar{\Xi}}(\xi,\bar{\xi}) = \frac{4}{\pi R_t^2} \cdot \begin{cases} \dfrac{\xi\bar{\xi}}{\sqrt{2R_c^2(\xi^2+\bar{\xi}^2) - (\xi^2-\bar{\xi}^2)^2 - R_c^4}} & \xi \in [0, R_t], \\ & \bar{\xi} \in [|\xi - R_c|, \xi + R_c] \\ 0 & \text{elsewhere} \end{cases} \tag{52}$$

The integration of (52) on all $\Xi$ values finally provides (18).

## Appendix B
## Proof of Proposition 4

Consider the transformation of r.v.s $(R_l, \Phi_l) \rightarrow (T_l, \Phi_l)$, from which, by inverting (24), one can obtain the inverse transformation from $T_l$ to $R_l$ as:

$$r_l(t_l, \phi_l, \phi_L) = \left[\frac{K_{\rm tx}\mathcal{G}(\phi_l, \phi_L)}{t_l} - 1\right]^{\frac{1}{\alpha}}. \tag{53}$$

Using (12) and evaluating the determinant of the Jacobian:

$$J = \begin{vmatrix} \dfrac{\partial r_l}{\partial \phi_l} & \dfrac{\partial r_l}{\partial t_l} \\ \dfrac{\partial \phi_l}{\partial \phi_l} & \dfrac{\partial \phi_l}{\partial t_l} \end{vmatrix}, \tag{54}$$

the joint pdf of $T_l$ and $\Phi_l$ given $\mathbf{V}$ can be evaluated by the method of transformation of r.v.s as:

$$\begin{aligned} f_{T_l,\Phi_l|\mathbf{V}}(t_l, \phi_l|\mathbf{v}) &= |J| \cdot f_{R_l,\Phi_l|\bar{\Xi},\bar{\Theta}}\left[r_l(t_l, \phi_l, \phi_L), \phi_l|\bar{\xi}, \bar{\theta}\right] \\ &= \frac{K_{\rm tx}}{\alpha\pi R_{\rm t}^2} \cdot \begin{cases} \dfrac{\mathcal{G}(\phi_l, \phi_L)}{t_l^2}\left[\dfrac{K_{\rm tx}\mathcal{G}(\phi_l, \phi_L)}{t_l} - 1\right]^{\frac{2}{\alpha}-1} & (t_l, \phi_l) \in \Delta_{\mathbf{v}} \\ 0 & \text{elsewhere} \end{cases} \end{aligned} \tag{55}$$

where $\Delta_{\mathbf{v}}$ is given by (27). The pdf of $T_l$ given $\mathbf{V}$ is the marginal of $T_l$ given $\mathbf{V}$ that can be calculated by integrating (55) over all $\Phi_l$ values belonging to $\Delta_{\mathbf{v},\Phi_l} = \{\phi_l : (t_l, \phi_l) \in \Delta_{\mathbf{v}}\}$. Thus:

$$f_{T_l|\mathbf{V}}(t_l|\mathbf{v}) = \int_{\Delta_{\mathbf{v},\Phi_l}} f_{T_l,\Phi_l|\mathbf{V}}(t_l, \phi_l|\mathbf{v}) \mathrm{d}\phi_l. \tag{56}$$

Substituting (55) in (56) one can finally obtain the pdf of $T_l$ given $\mathbf{V}$ in (26).

## Appendix C
## Proof of Proposition 5

Consider the r.v.s $\tilde{P}_1, \ldots, \tilde{P}_{L-1}$, which represent the (ascending) order statistics corresponding to the independent r.v.s $P_1, \ldots, P_{L-1}$. When $L < N_{\rm e} + 2$, no interference is present, since just one pair is active (IM case), or all interferers are suppressed (IS case).

When $L = N_{\rm e} + 2$, just one undesired source keeps interfering after the depletion of the $N_{\rm e}$ dofs, thus $P_{\rm I}$ is exactly given by the statistic of order $(L-1) - N_{\rm e} = 1$, and hence $P_{\rm I} = \tilde{P}_1 = \min\{P_1, \ldots, P_{L-1}\}$. Therefore, the pdf of $P_{\rm I}$ given $\mathbf{V}$ for $L = N_{\rm e}+2$ may be evaluated from [32, eq. 2.1.6], which provides exactly the first case in (30).

When $L > N_{\rm e}+2$, the two strongest undesired sources that keep interfering after the depletion of the $N_{\rm e}$ dofs are identified by the statistics of order $L - N_{\rm e} - 2$ and $L - N_{\rm e} - 1$, thus one may adopt the approximation $P_{\rm I} \cong \tilde{P}_{L-N_{\rm e}-2} + \tilde{P}_{L-N_{\rm e}-1}$. The conditional joint pdf of the two consecutive order statistics $\tilde{P}_{L-N_{\rm e}-2}$ and $\tilde{P}_{L-N_{\rm e}-1}$ can be derived from [32, eq. 2.2.1] according to (57), shown at the bottom of the page. Now, replacing $p_{l+1}$ by $p_{\rm I} - p_l$ in (57) and integrating on $p_l$, one obtains the second case in (30).

## Appendix D
## Proof of Proposition 6

The conditional r.v. $P_{\rm I}|\bar{\Xi}$ is given by the sum of $L-1$ independent and identically distributed conditional r.v.s $P_1|\bar{\Xi}, \ldots, P_{L-1}|\bar{\Xi}$, thus $\mathrm{E}[P_{\rm I}|\bar{\Xi}] = (L-1)\mathrm{E}[P_l|\bar{\Xi}]$. Besides, $P_l|\bar{\Xi}$ is given by the product of the two independent r.v.s $T_l|\bar{\Xi}$ and $Q_l$, where, according to (22), $\mathrm{E}[Q_l] = 1$. Hence, the mean conditional interference can be evaluated directly from the mean of $T_l|\bar{\Xi}$ as:

$$\mathrm{E}[P_{\rm I}|\bar{\Xi}] = (L-1)\mathrm{E}[T_l|\bar{\Xi}]. \tag{58}$$

For an infinitesimal beamwidth model of gain $\bar{\mathcal{G}}$, the pdf of $T_l$ given $\bar{\Xi}$ may be obtained recalling (3)-(6) for $0 \le \bar{\xi} \le R_{\rm t}$. This allows one to rewrite (26) as:

$$f_{T_l|\mathbf{V}}(t_l|\mathbf{v}) = f_{T_l|\bar{\Xi}}(t_l|\bar{\xi}) = \frac{K_{\rm tx}\bar{\mathcal{G}}}{\alpha\pi R_{\rm t}^2 t_l^2}\left(\frac{K_{\rm tx}\bar{\mathcal{G}}}{t_l} - 1\right)^{\frac{2}{\alpha}-1} \int_{\Delta_{\mathbf{v},\Phi_l}} \mathrm{d}\phi_l, \tag{59}$$

where $\Delta_{\mathbf{v},\Phi_l}$ is reported in (60), shown at the bottom of the page.

Consider first the case $\bar{\xi} = 0$. When $\bar{\xi} = 0$, (60) leads to $K_{\rm tx}\bar{\mathcal{G}}/(R_{\rm t}^{\alpha}+1) \le t_l \le K_{\rm tx}\bar{\mathcal{G}}$, which is independent of $\phi_l$. Hence, $\Delta_{\mathbf{v},\Phi_l} = \{\phi_l : (t_l, \phi_l) \in \Delta_{\mathbf{v}}\} = [0, 2\pi)$ and (59) becomes:

$$\begin{aligned} f_{T_l}(t_l) = {} & \frac{2K_{\rm tx}\bar{\mathcal{G}}}{\alpha R_{\rm t}^2 t_l^2}\left(\frac{K_{\rm tx}\bar{\mathcal{G}}}{t_l} - 1\right)^{\frac{2}{\alpha}-1} \\ & \cdot \left[u_1\left(t_l - \frac{K_{\rm tx}\bar{\mathcal{G}}}{R_{\rm t}^{\alpha}+1}\right) - u_0(t_l - K_{\rm tx}\bar{\mathcal{G}})\right]. \end{aligned} \tag{61}$$

Therefore, using (58) and (61), the mean interference at the center of $\mathcal{D}$ may be calculated as:

$$\mathrm{E}[P_{\rm I}^{\rm c}] = \frac{2K_{\rm tx}\bar{\mathcal{G}}(L-1)}{\alpha R_{\rm t}^2} \int_{\frac{K_{\rm tx}\bar{\mathcal{G}}}{R_{\rm t}^{\alpha}+1}}^{K_{\rm tx}\bar{\mathcal{G}}} \frac{1}{t_l}\left(\frac{K_{\rm tx}\bar{\mathcal{G}}}{t_l} - 1\right)^{\frac{2}{\alpha}-1} \mathrm{d}t_l, \tag{62}$$

which, after integration, provides (36).

$$f_{\tilde{P}_{L-N_{\rm e}-2},\tilde{P}_{L-N_{\rm e}-1}|\mathbf{V}}(p_l, p_{l+1}; L|\mathbf{v}) = \frac{F_{P_l|\mathbf{V}}^{L-N_{\rm e}-3}(p_l|\mathbf{v}) f_{P_l|\mathbf{V}}(p_l|\mathbf{v}) \bar{F}_{P_l|\mathbf{V}}^{N_{\rm e}}(p_{l+1}|\mathbf{v}) f_{P_l|\mathbf{V}}(p_{l+1}|\mathbf{v})}{\beta(L-N_{\rm e}-2, N_{\rm e}+2)} \tag{57}$$

$$\Delta_{\mathbf{v},\Phi_l} = \left\{\phi_l : \frac{K_{\rm tx}\bar{\mathcal{G}}}{\left|\sqrt{R_{\rm t}^2 - \bar{\xi}^2\sin^2(\phi_l - \bar{\theta})} - \bar{\xi}\cos(\phi_l - \bar{\theta})\right|^{\alpha} + 1} \le t_l \le K_{\rm tx}\bar{\mathcal{G}}, \phi_l \in [0, 2\pi)\right\} \tag{60}$$

Consider now the case $\bar{\xi} = R_{\rm t}$. When $\bar{\xi} = R_{\rm t}$, the first inequality in (60) can be analytically solved for $K_{\rm tx}\bar{\mathcal{G}}/[(2R_{\rm t})^{\alpha}+1] \le t_l \le K_{\rm tx}\bar{\mathcal{G}}$, thus identifying the set:

$$\Delta_{\mathbf{v},\Phi_l} = \left\{\phi_l : \chi(t_l) + \bar{\theta} \le \phi_l \le 2\pi - \chi(t_l) + \bar{\theta}\right\}, \quad (63)$$

where:

$$\chi(t_l) = \arccos\left[-\frac{1}{2R_{\rm t}}\left(\frac{K_{\rm tx}\mathcal{G}}{t_l} - 1\right)^{\frac{1}{\alpha}}\right]. \quad (64)$$

Using (63) in (59), one obtains:

$$f_{T_l}(t_l) = \frac{2K_{\rm tx}\bar{\mathcal{G}}}{\alpha R_{\rm t}^2 t_l^2}\left(\frac{K_{\rm tx}\bar{\mathcal{G}}}{t_l} - 1\right)^{\frac{2}{\alpha}-1}\left[1 - \frac{\chi(t_l)}{\pi}\right] \cdot \left\{u_1\left[t_l - \frac{K_{\rm tx}\bar{\mathcal{G}}}{(2R_{\rm t})^{\alpha}+1}\right] - u_0(t_l - K_{\rm tx}\bar{\mathcal{G}})\right\}. \quad (65)$$

This pdf does not provide an analytical form for the mean of $T_l$. However, for $x \le 0$, one may observe that $1 - \arccos(x)/\pi \lesssim 1/2 + x/\pi$. Hence, using this approximation and recalling (58), an upper bound for the mean interference at the boundary of $\mathcal{D}$ may be obtained as:

$$\mathrm{E}[P_{\rm I}^{\rm b}] \lesssim \frac{K_{\rm tx}\bar{\mathcal{G}}(L-1)}{\alpha R_{\rm t}^2} \int_{\frac{K_{\rm tx}\bar{\mathcal{G}}}{(2R_{\rm t})^{\alpha}+1}}^{K_{\rm tx}\bar{\mathcal{G}}} \frac{1}{t_l}\left(\frac{K_{\rm tx}\bar{\mathcal{G}}}{t_l} - 1\right)^{\frac{2}{\alpha}-1} \cdot \left[1 - \frac{1}{\pi R_{\rm t}}\left(\frac{K_{\rm tx}\bar{\mathcal{G}}}{t_l} - 1\right)^{\frac{1}{\alpha}}\right] \mathrm{d}t_l, \quad (66)$$

which, after integration, provides (37).

## Appendix E
## Transmission Capacity for an Homogeneous PPP of Intensity $\lambda$

Using the analysis of [33] for a homogeneous PPP, the cdf of the distance $R_l$ between the (centered) destination and the $l$-th closest interferer may be calculated as:

$$F_{R_l}^{\rm PPP}(r_l) = \frac{\gamma\left(l, \pi\lambda r_l^2\right)}{\Gamma(l)}\, u_1(r_l). \quad (67)$$

Remembering that $N_{\rm e}$ in (29) identifies the number of dofs available for interference suppression, the index $l = N_{\rm e} + 1$ identifies the nearest not suppressed interferer. Therefore, considering the average equivalent gain $\bar{\mathcal{G}}$, the interference power in absence of multipath-fading may be approximated as $p_{\rm I} \cong K_{\rm tx}\bar{\mathcal{G}}/(1 + r_{N_{\rm e}+1}^{\alpha})$ [11], and the corresponding cdf may be obtained as:

$$F_{P_{\rm I}}^{\rm PPP}(p_{\rm I}) = 1 - \frac{1}{\Gamma(N_{\rm e}+1)}\,\gamma\left[N_{\rm e}+1, \pi\lambda\left(\frac{K_{\rm tx}\bar{\mathcal{G}}}{p_{\rm I}} - 1\right)^{\frac{2}{\alpha}}\right] \cdot u_1(K_{\rm tx}\bar{\mathcal{G}} - p_{\rm I}). \quad (68)$$

Recalling the rules for the ratio between r.v.s [28], one may derive the cdf of the SIR $\rho = \bar{t}_L/p_{\rm I}$ using (68) and then the coverage probability for a SIR threshold $\omega$ as:

$$\eta^{\rm PPP}(\omega, \lambda) = 1 - \frac{1}{\Gamma(N_{\rm e}+1)}\,\gamma\left[N_{\rm e}+1, \pi\lambda\left(\frac{K_{\rm tx}\bar{\mathcal{G}}\omega}{\bar{t}_L} - 1\right)^{\frac{2}{\alpha}}\right] \cdot u_1(K_{\rm tx}\bar{\mathcal{G}}\omega - \bar{t}_L). \quad (69)$$

Finally, adopting the original definition in [6], the transmission capacity in the presence of a homogeneous PPP when the Shannon bound is adopted may be evaluated as:

$$c^{\rm PPP}(\varepsilon, \omega) = \log_2(1+\omega)(1-\varepsilon)\sup\left\{\lambda : \eta^{\rm PPP}(\omega, \lambda) \ge 1-\varepsilon\right\}. \quad (70)$$

## References


[1] *IEEE Draft Standard for Information Technology—Telecommunications and Information Exchange Between Systems—Local and Metropolitan Area Networks—Specific Requirements—Part 11: Wireless LAN Medium Access Control (MAC) and Physical Layer (PHY) Specifications—Amendment 4: Enhancements for Very High Throughput for Operation in Bands Below 6 GHz*, IEEE Standard 802.11ac, Jan. 2014.

[2] A. Zanella and M. Zorzi, "Theoretical analysis of the capture probability in wireless systems with multiple packet reception capabilities," *IEEE Trans. Commun.*, vol. 60, no. 4, pp. 1058–1071, Apr. 2012.

[3] D. S. Chan, T. Berger, and L. Tong, "Carrier sense multiple access communications on multipacket reception channels: Theory and applications to IEEE 802.11 wireless networks," *IEEE Trans. Commun.*, vol. 61, no. 1, pp. 266–278, Jan. 2013.

[4] M. Hasan, E. Hossain, and D. Niyato, "Random access for machine-to-machine communication in LTE-advanced networks: Issues and approaches," *IEEE Commun. Mag.*, vol. 51, no. 6, pp. 86–93, Jun. 2013.

[5] S. P. Weber, X. Yang, J. G. Andrews, and G. de Veciana, "Transmission capacity of wireless ad hoc networks with outage constraints," *IEEE Trans. Inf. Theory*, vol. 51, no. 12, pp. 4091–4102, Dec. 2005.

[6] S. P. Weber, J. G. Andrews, X. Yang, and G. de Veciana, "Transmission capacity of wireless ad hoc networks with successive interference cancellation," *IEEE Trans. Inf. Theory*, vol. 53, no. 8, pp. 2799–2814, Aug. 2007.

[7] V. Mordachev and S. Loyka, "On node density—Outage probability tradeoff in wireless networks," *IEEE J. Sel. Areas Commun.*, vol. 27, no. 7, pp. 1120–1131, Sep. 2009.

[8] P. C. Pinto and M. Z. Win, "Communication in a Poisson field of interferers—Part I: Interference distribution and error probability," *IEEE Trans. Wireless Commun.*, vol. 9, no. 7, pp. 2176–2186, Jul. 2010.

[9] P. C. Pinto and M. Z. Win, "Communication in a Poisson field of interferers—Part II: Channel capacity and interference spectrum," *IEEE Trans. Wireless Commun.*, vol. 9, no. 7, pp. 2187–2195, Jul. 2010.

[10] K. Gulati, R. K. Ganti, J. G. Andrews, B. L. Evans, and S. Srikanteswara, "Characterizing decentralized wireless networks with temporal correlation in the low outage regime," *IEEE Trans. Wireless Commun.*, vol. 11, no. 9, pp. 3112–3125, Sep. 2012.

[11] Z. Gong and M. Haenggi, "Interference and outage in mobile random networks: Expectation, distribution, and correlation," *IEEE Trans. Mobile Comput.*, vol. 13, no. 2, pp. 337–349, Feb. 2014.

[12] M. Di Renzo and P. Guan, "A mathematical framework to the computation of the error probability of downlink MIMO cellular networks by using stochastic geometry," *IEEE Trans. Commun.*, vol. 62, no. 8, pp. 2860–2879, Aug. 2014.

[13] A. Guo and M. Haenggi, "Spatial stochastic models and metrics for the structure of base stations in cellular networks," *IEEE Trans. Wireless Commun.*, vol. 12, no. 11, pp. 5800–5812, Nov. 2013.

[14] W. Lu and M. Di Renzo, "Stochastic geometry modeling of cellular networks: Analysis, simulation and experimental validation," in *Proc. 18th ACM Int. Conf. MSWiM*, 2015, pp. 179–188.

[15] H. Inaltekin, M. Chiang, H. V. Poor, and S. B. Wicker, "On unbounded path-loss models: Effects of singularity on wireless network performance," *IEEE J. Sel. Areas Commun.*, vol. 27, no. 7, pp. 1078–1092, Sep. 2009.

[16] R. K. Ganti and M. Haenggi, "Interference and outage in clustered wireless ad hoc networks," *IEEE Trans. Inf. Theory*, vol. 55, no. 9, pp. 4067–4086, Sep. 2009.

[17] S. Srinivasa and M. Haenggi, "Distance distributions in finite uniformly random networks: Theory and applications," *IEEE Trans. Veh. Technol.*, vol. 59, no. 2, pp. 940–949, Feb. 2010.
[18] R. K. Ganti, J. G. Andrews, and M. Haenggi, "High-SIR transmission capacity of wireless networks with general fading and node distribution," *IEEE Trans. Inf. Theory*, vol. 57, no. 5, pp. 3100–3116, May 2011.
[19] F. Babich and M. Comisso, "Multi-packet communication in heterogeneous wireless networks adopting spatial reuse: Capture analysis," *IEEE Trans. Wireless Commun.*, vol. 12, no. 10, pp. 5346–5359, Oct. 2013.
[20] V. Naghshin, A. M. Rabiei, N. C. Beaulieu, and B. Maham, "Accurate statistical analysis of a single interference in random networks with uniformly distributed nodes," *IEEE Commun. Lett.*, vol. 18, no. 2, pp. 197–200, Feb. 2014.
[21] K. V. Mardia and P. E. Jupp, *Directional Statistics*. New York, NY, USA: Wiley, 2000.
[22] S. R. Jammalamadaka and A. Sengupta, *Topics in Circular Statistics*. London, U.K.: World Scientific, 2001.
[23] P. Petrus, J. H. Reed, and T. S. Rappaport, "Geometrical-based statistical macrocell channel model for mobile environments," *IEEE Trans. Commun.*, vol. 50, no. 3, pp. 495–502, Mar. 2002.
[24] C. A. Balanis, *Antenna Theory: Analysis and Design*. New York, NY, USA: Wiley, 1997.
[25] V. Erceg *et al.*, *TGn Channel Models*, IEEE Standard 802.11-03/940r4, 2004.
[26] K. I. Pedersen, P. E. Mogensen, and B. H. Fleury, "A stochastic model of the temporal and azimuthal dispersion seen at the base station in outdoor propagation environments," *IEEE Trans. Veh. Technol.*, vol. 49, no. 2, pp. 437–447, Mar. 2000.
[27] F. Babich and M. Comisso, "Throughput and delay analysis of 802.11-based wireless networks using smart and directional antennas," *IEEE Trans. Commun.*, vol. 57, no. 5, pp. 1413–1423, May 2009.
[28] R. D. Yates and D. J. Goodman, *Probability and Stochastic Processes*. New York, NY, USA: Wiley, 1999.
[29] M. Haenggi and R. K. Ganti, "Interference in large wireless networks," *Found. Trends Netw.*, vol. 3, no. 2, pp. 127–248, 2009.
[30] M. Abramowitz and I. A. Stegun, Eds., *Handbook of Mathematical Functions: With Formulas, Graphs, and Mathematical Tables* (Applied Mathematics), ser. 55. Gaithersburg, MD, USA: NBS, 1964.
[31] R. E. Walpole, R. H. Myers, S. L. Myers, and K. Ye, *Probability and Statistics for Engineers and Scientists*. Upper Saddle River, NJ, USA: Pearson Education, 2007.
[32] H. A. David and H. N. Nagaraja, *Order Statistics*. Hoboken, NJ, USA: Wiley, 2003.
[33] H. R. Thompson, "Distribution of distance to Nth neighbour in a population of randomly distributed individuals," *Ecology*, vol. 37, no. 2, pp. 391–394, Apr. 1956.

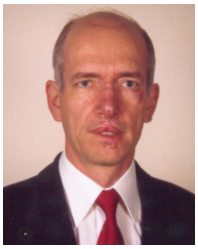

**Fulvio Babich** (SM'03) received the doctoral degree in electrical engineering from the University of Trieste, in 1984. From 1984 to 1987, he was with the Research and Development Department, Telettra, where he was involved in optical communications. He was with Zeltron (Electrolux Group) as the Company Head of the Home System European projects. In 1992, he joined the Department of Electrical Engineering, now converged in the Department of Engineering and Architecture, University of Trieste, where he is currently an Associate Professor of digital communications and telecommunication networks. He served as the Co-Chair of the Communication Theory Symposium, ICC 2005, Seoul, of the Wireless Communication Symposium, ICC 2011, Kyoto, of the Wireless Communication Symposium, WCSP 2012, Huangshan, China, and of the Communication Theory Symposium, ICC 2014, Sidney. He has been a member of the Directive Board of CNIT (National Inter-University Consortium for Telecommunications, a non-profit consortium among 37 Italian universities, whose main purpose is to coordinate and foster basic and applied research).

**Massimiliano Comisso** (M'09) received the Laurea degree in electronics engineering and the Ph.D. degree in information engineering from the University of Trieste, Italy. He was with Alcatel, where he worked on DWDM communication systems, and collaborated with Danieli Automation on electromagnetic NDE techniques. He is an Assistant Professor with the Department of Engineering and Architecture, University of Trieste. He has authored or co-authored over 50 international scientific papers, and serves as a Reviewer/TPC Member for several IEEE journals and conferences. His research interests involve smart antenna systems, distributed wireless networks, antenna array synthesis, and small antennas. He was the Best Student Paper Award finalist at GLOBECOM 2006 and received the Best Paper Award at CAMAD 2009.